Geophysical Journal International

Geophys. J. Int. (2022) **229,** 1567–1585
Advance Access publication 2022 January 28
GJI Geodynamics and Tectonics

https://doi.org/10.1093/gji/ggac016

Timing of Eocene compressional plate failure during subduction initiation, northern Zealandia, southwestern Pacific

W.R. Stratford [1], R. Sutherland,[2] G.R. Dickens,[3] P. Blum,[4] J. Collot,[5] M. Gurnis,[6] S. Saito,[7] A. Bordenave,[8] S.J.G. Etienne,[5] C. Agnini,[9] L. Alegret,[10] G. Asatryan,[11] J. Bhattacharya [12], L. Chang,[13] M.J. Cramwinckel,[14] E. Dallanave,[15] M.K. Drake,[16] M. Giorgioni,[17] D.T. Harper,[16] H.-H.M. Huang,[18] A.L. Keller,[19] A.R. Lam,[20] H. Li,[21] H. Matsui,[22] H.E.G. Morgans,[1] C. Newsam,[21,23] Y.-H. Park,[22,24] K.M. Pascher,[1] S.F. Pekar,[25] D.E. Penman,[26] T. Westerhold[27] and X. Zhou[28]

[1] *GNS Science, Lower Hutt, 5011, New Zealand. E-mail: w.stratford@gns.cri.nz*
[2] *School of Geography, Environment and Earth Sciences, Victoria University of Wellington, Wellington, 6012, New Zealand*
[3] *School of Natural Sciences, Trinity College Dublin, The University of Dublin, Dublin 2, Ireland*
[4] *Department of Geology, University of Kansas, Lawrence, Kansas 66045, USA*
[5] *Geological Survey of New Caledonia, (SGNC), 98845, Noumea, New Caledonia*
[6] *Division of Geological and Planetary Sciences, California Institute of Technology, Pasadena, CA, California 91125 USA*
[7] *Institute for Marine-Earth Exploration and Engineering (MarE3), Japan Agency for Marine-Earth Science and Technology, Yokosuka, Kanagawa 237-0061, Japan*
[8] *Université Bordeaux Montaigne/EA* 4592 *Géoressources and Environnement,* 1 *allée Fernand Daguin,* 33607 *Pessac cedex, France*
[9] *Department of Geosciences, Università degli Studi di Padova, 2 - 35122 Padova, Italy*
[10] *Department of Earth Sciences, Universidad de Zaragoza, 50009 Zaragoza, Spain*
[11] *Museum für Naturkunde, Leibniz-Institut für Evolutions und Biodiversitätsforschung, 10115 Berlin, Germany*
[12] *School of Geosciences, Mewbourne College of Earth and Energy. University of Oklahoma, Norman, OK 73019, USA*
[13] *School of Earth and Space Sciences, Peking University, Beijing* 100871, *China*
[14] *National Oceanography Centre Southampton, University of Southampton, Southampton SO14 3ZH, UK*
[15] *Faculty of Geosciences, University of Bremen, 28334 Bremen, Germany*
[16] *Ocean Science Department, University of California, Santa Cruz, California 95064, USA*
[17] *Institute of Geosciences, Universidade de Brasília, Brasilia 70910-900, Brazil*
[18] *Paleobiology Department, National Museum of Natural History, Smithsonian Institution, Washington, D.C. 20560, USA*
[19] *Department of Earth Sciences, University of California, Riverside, California 92521, USA*
[20] *Department of Geological Sciences and Environmental Studies, Binghamton University, Binghamton NY 13902-6000, USA*
[21] *Institute of Oceanology, Chinese Academy of Sciences, Qingdao 266071, China*
[22] *Centre for Advanced Marine Core Research Kochi University, Kochi 783-8502, Japan*
[23] *Department of Earth Sciences, University College London, London WC1E 6BS, United Kingdom (currently at: Network Stratigraphic Consulting Ltd, Potters Bar, EN6 3JF, United Kingdom)*
[24] *Marine Research Institute, Pusan National University, Busan 46241, Republic of Korea*
[25] *School of Earth and Environmental Sciences, Queens College (CUNY), Queens, NY 11367, USA*
[26] *Department of Geosciences, Utah State University, Logan UT 84322-4505, USA*
[27] *Centre for Marine and Environmental Sciences, University of Bremen, D-28334 Bremen, Germany*
[28] *Department of Marine and Coastal Sciences, Rutgers, The State University of New Jersey, NJ 08901-8520, USA*

Received 2021 December 13

SUMMARY

Rapid onset of subduction tectonics across the western Pacific convergent margins in the early Eocene was followed by a slower phase of margin growth of the proto Tonga-Kermadec subduction system north of Zealandia during a middle Eocene phase of tectonic adjustment. We present new age constraints from International Ocean Discovery Program Expedition 371 borehole data on deformation events in northern Zealandian sediments that document the formation of the convergent margin boundary northwest of New Zealand. The deformation shows a shortening event that lasted up to 20 myr and acted over distances of ∼1000 km inboard of the evolving plate margin, just northwest of New Zealand. Multichannel seismic profiles tied to our new borehole sites show shortening occurred predominantly between 45 and 35 Ma with some deformation related to slope failure continuing into the Oligocene. The

termination of shortening is linked to opening of the backarc basins of the southwest Pacific and the migration of the Tonga-Kermadec Trench to the east which may have removed the structural evidence of the Eocene plate margin. Palaeogene deformation observed inboard of the evolving proto Tonga-Kermadec subduction system indicates that the lithosphere of northern Zealandia, a region of thin continental crust, was strong enough to act as a stress guide. Compressive stresses that caused intraplate folding and faulting developed behind the initiating subduction system with the finite period of deformation indicating the time frame over which an active convergent margin lay along the northern margin of Zealandia.

Key words: New Zealand; Pacific Ocean; Continental margins: convergent; Intra-plate processes; Subduction zone processes.

1 INTRODUCTION

Subduction initiation studies often address the roles plate buoyancy and pre-existing tectonics play using 2-D computational models of plate boundary evolution (Leng & Gurnis 2011; Stern & Gerya 2018). Fewer studies have addressed the evolution of a subduction zone to understand the along margin, 3-D growth of a convergent plate boundary (Zhou et al. 2018). Current views of plate tectonics in the north-western Pacific suggest that subduction initiation was rapid (Arculus et al. 2015; Ishizuka et al. 2018; Li et al. 2021) and was associated with the change in Pacific plate motion around 50 Ma, which can be deduced from global plate circuits and hotspot tracks (Whittaker et al. 2007; Müller et al. 2016; Torsvik et al. 2017). Evidence from forearc volcanic rocks indicate that once established, subducted slabs drove further lateral expansion of western Pacific subduction zones (Meffre et al. 2012) and formation of new subduction zones, which continued into the Miocene (Wood et al. 2000). Eventually, a state of self-sustaining subduction is reached and the negative buoyancy of the slab continues to drive the system (Gurnis et al. 2004).

Lateral subduction propagation direction and rate may be revealed by along arc variations in geochemistry and age of arc and forearc rocks (Ozawaa et al. 2004; Meffre et al. 2012). For example, similar ages of volcanic rocks along the Izu-Bonin-Mariana forearc indicate subduction initiated rapidly, perhaps by a margin collapse event (Arculus et al. 2015; Ishizuka et al. 2018; Mauder et al. 2020) whereas a progression in rock ages along the Andes (Chen et al. 2019) and Tonga-Kermadec arcs suggest longer periods of lateral growth (Meffre et al. 2012). Temporal relationships between marginal and intraplate deformation events observed behind a subduction zone may also elucidate rates of lateral propagation and mode of subduction initiation (Lewis & Hayes 1983) with convergent and divergent deformation predicted by numerical models of induced and spontaneous subduction initiation, respectively (Gurnis et al. 2004; Stern 2004; Stern & Gerya 2018). In places this deformation may be the only evidence remaining of subduction zone evolution, as growth of backarc basins and extended periods of volcanism can displace and overprint original arc and forearc structures.

Observations of intraplate shortening can be used to constrain the strength of the lithosphere and the nature of the plate boundaries producing the stress, even after these boundaries have become extinct, overprinted or removed from the geological record (Lambeck 1983). The effectiveness of transferring stress to large distances behind a convergent margin and across structural boundaries depends on the rheology of the lithosphere which varies with crustal thickness, composition and thermal state (Raimondo et al. 2014). A strong lithospheric mantle may act as a stress guide transferring stress into the interior while still permitting shortening in the brittle crust at structural boundaries (Handy & Brun 2004; Burov & Watts 2006; Burov 2010).

In this study, we use information from International Ocean Discovery Program (IODP) Expedition 371 boreholes (Sutherland et al. 2019, Fig. 1) to date deformation events observed in northern Zealandian sediments that are evidence for a ∼1000 km wide and ∼20 myr long period of deformation that occurred behind the Tonga-Kermadec subduction zone during its propagation southward across northern Zealandia. Remnants of the Eocene plate boundary to the north west of New Zealand have yet to be located and may have been partly or entirely translated to the east by opening of southwest Pacific backarc basins. Dating deformation that can be linked to plate boundary evolution in the Eocene is pertinent to understanding the early phases of the Tonga-Kermadec subduction system as few volcanic arc rocks from this time period have been found in the region (Mortimer et al. 2007).

2 TECTONIC SETTING

Northern Zealandia comprises a series of lengthy ridges and basins that formed during Gondwana breakup (Uruski 2010) (Fig. 1). Zealandia underwent extension from 100 to 85 Ma (Bradshaw 1989), and separated from Australia through seafloor spreading in the Tasman Sea from 85 to 52 Ma (Gaina et al. 1998). A network of multichannel seismic lines across the region reveal deformation that postdates these major plate tectonic events and is middle Eocene to Oligocene in age (Bache et al. 2012; Sutherland et al. 2020).

The Tonga-Kermadec subduction zone initiated near New Caledonia in the Eocene (Crawford et al. 2003; Meffre et al. 2012; Dallanave et al. 2018). Linked to changes in Pacific plate motion (Whittaker et al. 2007) signified by the ∼47 Ma bend in the Emperor-Hawaii seamount chain (Torsvik et al. 2017), and evidenced by subduction-related Eocene basalts and younger volcanic rocks dredged from the present day Tonga forearc, the subduction zone has rotated and translated eastward since inception (Meffre et al. 2012). Eocene changes in Australian plate motion are indicated by the onset of rapid seafloor spreading south of Australia and New Zealand at ∼45 Ma (Sutherland 1995; Cande & Stock 2004). Oblique convergence or southwest dipping subduction north of Reinga Basin in the middle Eocene is inferred from studies of stratigraphic records (Bache et al. 2012), whereas plate tectonic reconstructions model this as a transform boundary (Schellart & Spakman 2012) or as part of a northeast dipping subduction system linking New Caledonia and New Zealand (Crawford et al. 2003; Schellart 2006; Whattam et al. 2008).

Crustal thickness measurements in Northern Zealandia are sparse, but wide-angle seismic models indicate they range from

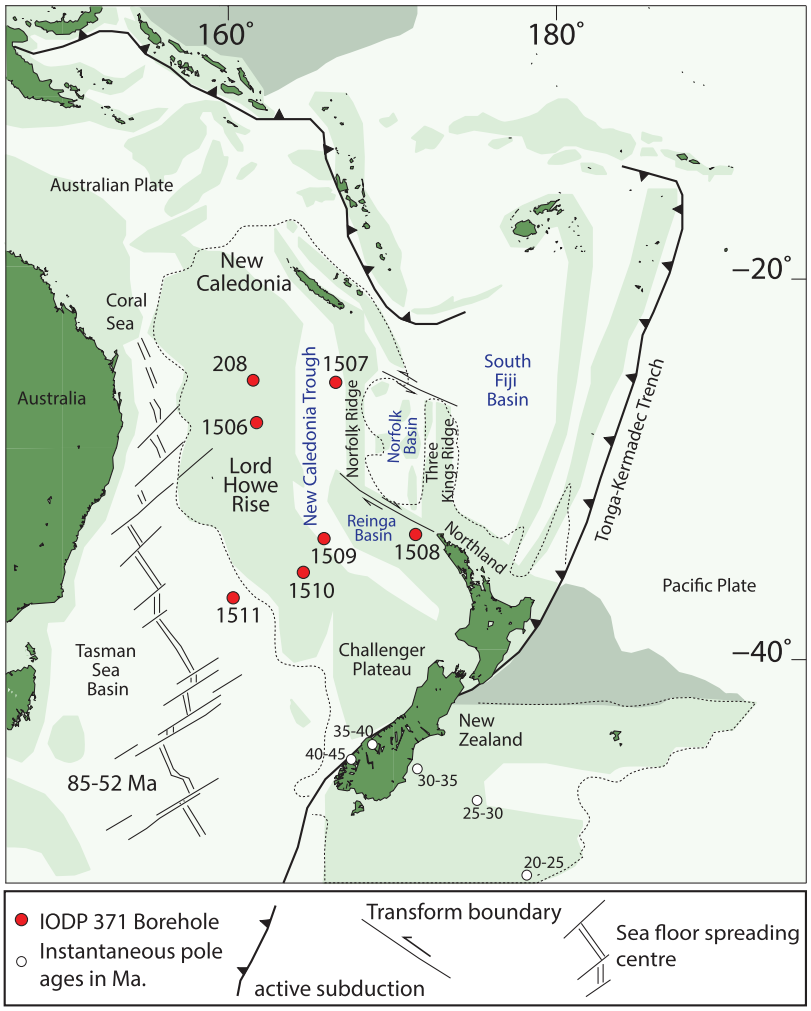

Figure 1. Location map for northern Zealandia showing main structural elements and IODP 371 borehole locations. Red circles are IODP Expedition 371 (1506–1511) and DSDP (208) boreholes. White circles show the movement of the Australia-Pacific instantaneous pole with time (Sutherland 1995). Dashed lines outline the largely submerged continent of Zealandia. Northern Zealandia is the region of thin continental crust west and north of New Zealand. Light green shading shows submarine regions that are elevated (predominantly thin continental crust), mid green shaded blocks are oceanic plateau and dark green shading shows subaerial regions.

23 km on the Northern Lord Howe Rise (Klingelhoefer et al. 2007; Gallais et al. 2019) to ∼8 km in the New Caledonia Trough (Klingelhoefer et al. 2007)). The region is below the influence of surface currents, but above the carbonate compensation depth (CCD), and has accumulated a fossil-rich, near-continuous pelagic sediment record since the Palaeogene with the oldest sediments sampled being Late Cretaceous (Deep Sea Drilling Program [DSDP] Site 208, Leg 21, Burns et al. 1973). These sediments provide a record in which to date regional tectonic deformation that can be linked to a major change in plate motion in the Eocene. The boreholes of IODP Expedition 371 (Sutherland et al. 2019) were drilled and cored to date this deformation.

3 DATA AND ANALYSIS

Site survey investigations leading up to IODP Expedition 371 collected multichannel seismic data in a grid of crossing lines at the planned borehole sites. Data were collected on the Tan1409 voyage for all sites except for Site U1508 in Reinga Basin, where an established grid of high-quality data was already available. The site survey data were used to find optimum sites to sample Palaeogene deformation that had previously been identified on reconnaissance seismic lines (Bache et al. 2012; Bache et al. 2014).

A total of 3729 m of sediment was drilled with 2506 m of core recovered on IODP Expedition 371 at six borehole sites (Fig. 1). A full description of data and methods can be found in the Expedition 371 proceeding volume (Sutherland et al. 2019). Depositional environments across the boreholes range from abyssal to upper bathyal and proximity to landmasses varies (Fig. 1) which is reflected in the variable composition of the sediments cored. Sediments sampled include deep to shallow bathyal carbonate, which contain various amounts of chert and siliceous fossils in the Eocene. Clay and volcanic sand were cored near volcanic edifices and Cretaceous to Palaeocene bathyal marine claystone was cored in the southern New Caledonia Trough indicating a phase of sediment supply from land nearby. Abyssal clay and diatomite were cored in the Tasman Sea Basin above a basement of oceanic crust. The boreholes contained sediments that are confirmed to be Palaeogene in age (Sutherland et al. 2019). Cores are

dated using the Geologic Time Scale 2012 (GTS2012) age model for magnetic polarity reversals, nannofossils, planktic foraminifera and radiolarians and, where present, dinocysts (Gradstein et al. 2012).

3.1 Borehole ties to multichannel seismic profiles

Physical properties measured on the cores and wireline logs measured downhole are used to construct impedance (product of velocity and density) with depth profiles for each of the borehole sites (Figs 2 and 3a–8a). Impedance values are used to construct synthetic seismograms for comparison to multichannel seismic traces extracted at the borehole sites (Figs 3a and b–8a and b). Correlation of the synthetic trace with the seismic trace data links core physical properties, lithology and sediment ages (determined from microfossils) to reflections in the seismic trace data. Age constraints from the boreholes can then be used to date the deformation events observed in the wider multichannel seismic data.

Corrections for porosity rebound are usually applied to measurements made on cores to adjust physical properties measurements to *in situ* values (Urmos & Wilkens 1993) and obtain a better fit between core measured values and seismic velocities from multichannel data. Previously, Stratford et al. (2018) used the Urmos & Wilkens (1993) carbonate rebound solution to create synthetic velocity profiles for DSDP boreholes cores in northern Zealandia. Applying this solution to the IODP Expedition 371 laboratory measured velocities produces a synthetic solution that is a poor fit to the multichannel seismograms. A simpler method was therefore used to tie borehole physical properties to seismic data, where percentage changes are applied to *P*-wave velocity measurements (Fig. 2). Due to differences in recovery, deformation, drilling method and seismic data characteristics at each site, the measured *P*-wave velocities require site specific adjustments.

Density values are either left unaltered or modelled as a smooth profile with depth as they only effect reflection amplitudes. Core measurements are made at a significantly larger spacing (metre scale) than the wireline measurements (mm scale) and, as such, core measurements are more likely to contain sample bias. An impedance (velocity × density) profile with depth is calculated for each borehole (Figs 2 and 3a–8a). The reflectivity method (Pirera & Zanzi 1993) is used to calculate a synthetic seismogram from this profile. The input source is a Ricker wavelet (Ricker 1943) with a period of 10 ms. The output synthetic trace is bandpass filtered to match the frequency content of the seismic trace data (Figs 3b–8b). As velocity-depth measurement spacings and coverage vary, best-fitting solutions for each borehole are found by matching the two-way traveltimes of prominent reflectors. As seismic velocities predominantly increase with depth, rarer negative polarity reflections (low velocity zones) are useful for providing confidence in the fit to the data. The corrections applied to each borehole to produce the final velocity–density pairs are listed by site below. Velocity/density data and synthetic seismic models for the borehole sites can be downloaded from the data repository (see Data availability).

3.1.1. Site U1506

The seafloor and volcanic basement reflectors at Site U1506 are used to constrain the impedance with depth profile (Figs 2 and 3c). Observed seismic reflectivity between these two horizons is low amplitude (Figs 3c and f) and cannot be replicated with confidence using the synthetic seismic trace. Core-measured *P*-wave velocities in the sedimentary section are increased by 8 per cent to fit the two-way-time (TWT) between the two reflectors. This site was rotary drilled, and core measured velocities are likely affected by both porosity rebound and drilling disturbance. Velocity corrections are not applied to volcanic basement measurements.

3.1.2. Site U1507

Site U1507 was logged for *P*-wave velocity and density between 70 and 840 m depth. The density values are interpolated at wireline *P*-wave velocity (*Vp*) depth measurement sites for impedance calculations (Figs 2 and 4a). To improve the fit between synthetic and seismic trace data, the wireline velocities are reduced by 1 per cent. The best-fitting solution for correcting the core data in the top 70 m of the borehole was achieved by applying a standard carbonate rebound correction (Urmos & Wilkens 1993).

3.1.3. Site U1508

As the bore hole at Site U1508 was susceptible to collapse, the density tool was not included in the wireline logging tool and a smoothed density profile based on core density values was used to calculate impedance (Figs 2 and 5). The best-fitting synthetic solution is calculated by decreasing the wireline logged *P*-wave velocities by 5 per cent. The top 80 m and the bottom 45 m of the borehole were not logged so core measurements are used with the same percentage decrease in *Vp* applied. Confidence in the fit of the model to the trace data is provided by matching the TWTs of two unconformities observed in the seismic data and the core at 321 and 379 m depth (Fig. 5).

3.1.4. Site U1509

At Site U1509 core measured velocities and densities are used to calculate impedance down the borehole (Fig. 2). Densities are interpolated at velocity measurement positions. An early Eocene limestone layer in the core coincides with a significant increase in velocity and density values and is interpreted as the source of a strong positive reflection on the seismic data at 4.3 s TWT (Fig. 6f). This layer is used as a pinning point for the borehole tie to seismic model. A good fit to the TWT to the limestone reflector and a tentative match to a 4.5 s TWT reflector in Palaeocene claystone can be achieved by increasing *P*-wave velocity by 3 per cent.

3.1.5. Site U1510

Physical property measurements from the core from Site U1510 are used to calculate an impedance profile for the borehole (Figs 2e and 7a). Density values are interpolated at velocity measurement positions. Sediments at Site U1510 were disturbed by drilling and the cores were crushed in places. Good recovery of core was achieved in the top 140 m in Miocene sediment, but below this the Eocene sediments are silica rich, contain chert fragments and recovery was poor. Recovery improved below 350 m depth but remained poor compared to the other Expedition 371 boreholes. Although numerous chert fragments were recovered between 140 and 350 m, the seismic data between 1.8 and 2.1 s TWT has low reflectivity indicating that the chert layers are too thin to produce distinct reflections (Fig. 7f). The chert fragments have high *Vp* and density and the increase in *P*-wave velocities required to produce a synthetic solution for this section of the core indicates that the chert layers may be

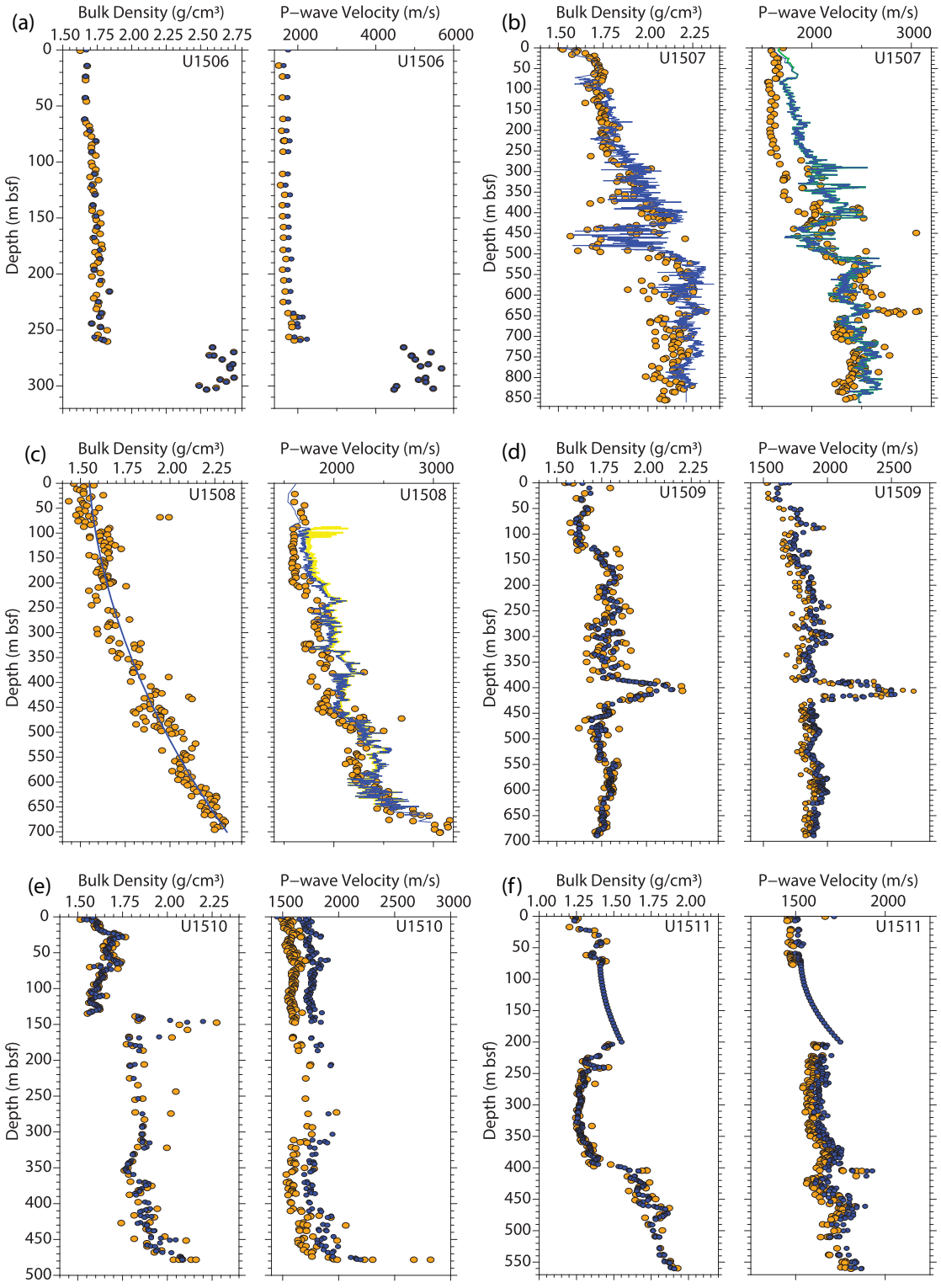

Figure 2. Bulk density and *P*-wave velocity data from IODP Expedition 371 boreholes. Orange data points are raw density and velocity measurements made on the core in the ship laboratory. Blue data points (core) and lines (wireline or interpreted) are the input values for the synthetic trace calculation. (a) Site U1506: the cluster of high density and velocity values at the base of the borehole ~270 m are from volcanic rocks. (b) Site U1507: green is the raw wireline velocity model. Blue is the final model (wireline + core measurements for the top 70 m, velocity and density). (c) Site U1508: core density measurements (orange circles) are interpolated at the wireline data point locations to use in the synthetic model (blue line). The yellow velocity profile is raw wireline velocities, and the blue is the final synthetic model. (d) Site U1509, (e) Site U1510. (f) Site U1511: note the drilled section of the borehole has inferred velocities and densities calculated during the construction of the synthetic model by using the travel time between two reflectors.

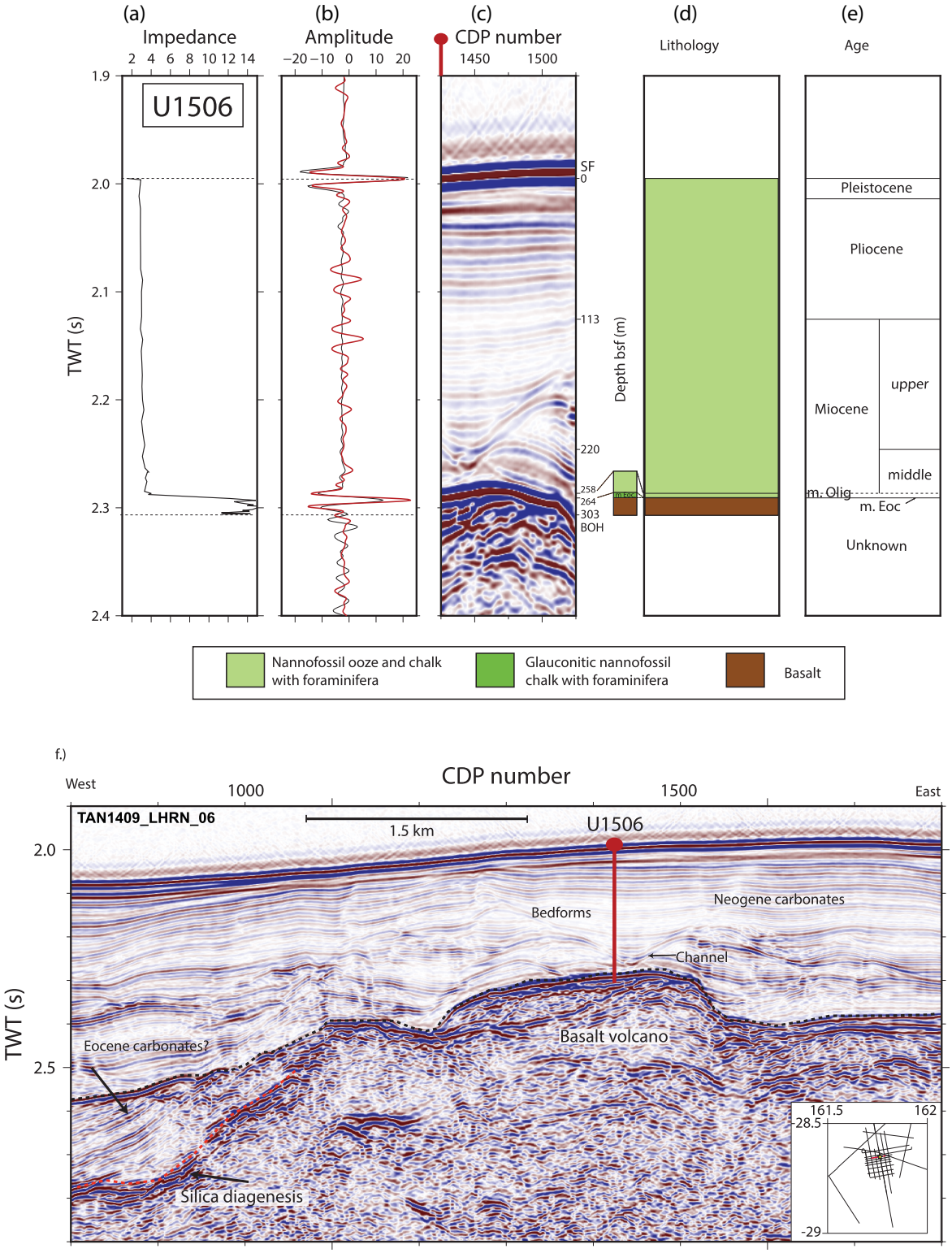

Figure 3. Borehole ties to seismic and timing of tectonic events at Site U1506. (a) Impedance (velocity × density) plotted against TWT for the borehole using the data shown in Fig. 2. This impedance model is used to produce the synthetic seismic trace (red) in (b). (b) Synthetic solution for the borehole (in TWT) plotted against real seismic trace data extracted from the borehole site. (c) Sample of seismic data near the borehole showing the seismic characteristics at the borehole site (right axis is marked as depth bsf in metres). Red marker at top of plot shows location of the borehole. BOH is bottom of hole. SF is seafloor. (d) Lithologic interpretation. (e) Geological timescale interpreted from the fossil assemblage and palaeomagnetic data of the core. (f) Seismic section showing geological structure near the borehole. Red marker shows the location and depth of the borehole. Labels indicate interpreted stratigraphic and tectonic horizons. Inset shows the site survey and regional seismic lines used to determine structure in vicinity of the borehole. Red line shows the location of the seismic data shown in main figure. Yellow star is the borehole site.

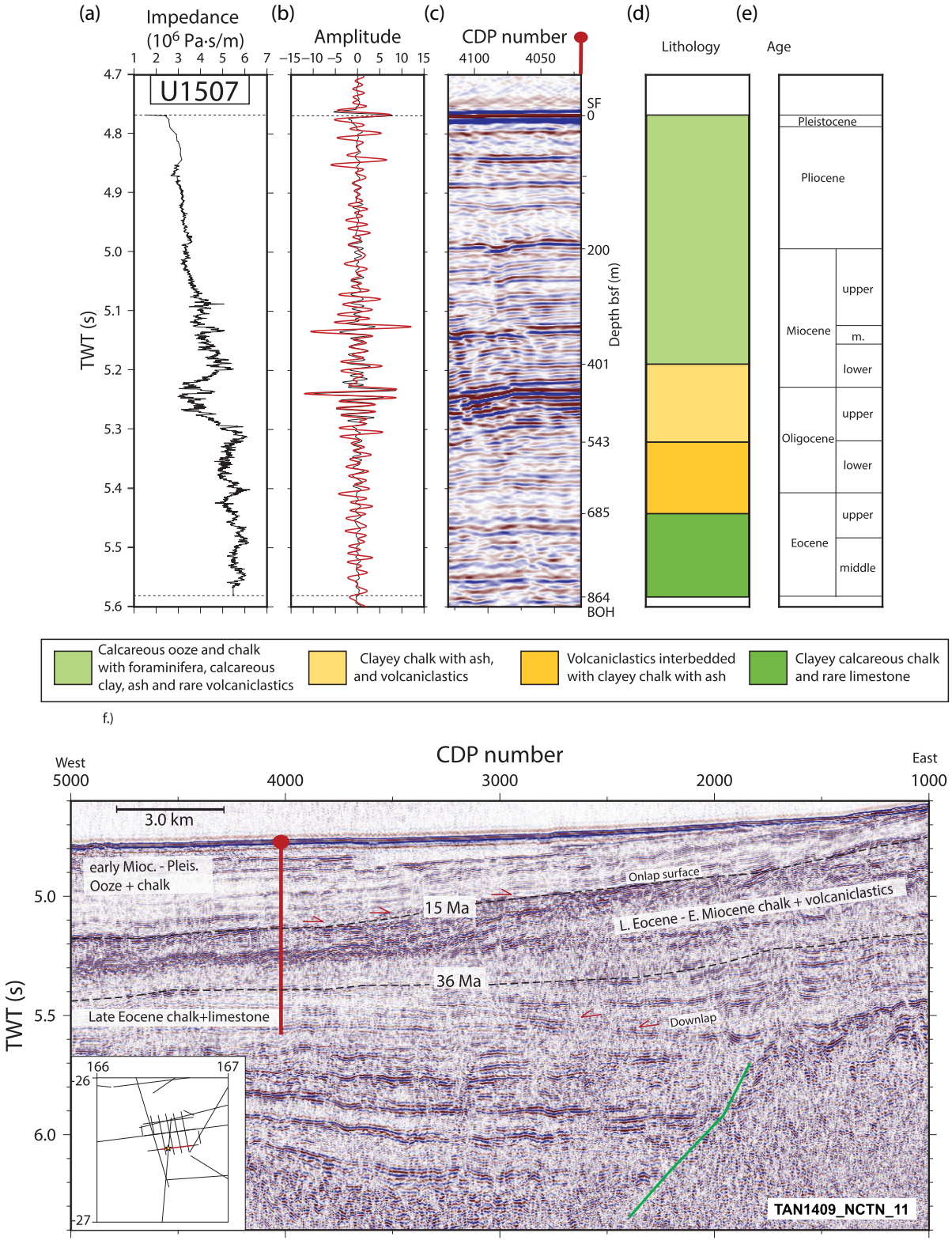

Figure 4. Borehole ties to seismic and timing of tectonic events at Site U1507. See the caption for Fig. 3 for further explanation. Red arrows show direction of onlap and downlap for sediments. Green line is inferred fault trace.

numerous. Drilling through interbedded hard (chert) and soft (chalk) layers may account for the low recovery. A 10 per cent increase in *Vp* produces a reasonable fit between seismic trace and synthetic data. Confidence in the model is provided by matching the strong reflector at 138 m depth associated with the onset of silicification of the sediments and a disrupted layer that can be traced laterally to lava flows on the adjacent volcano with volcanoclastic deposits that occur at 415 m depth in the core.

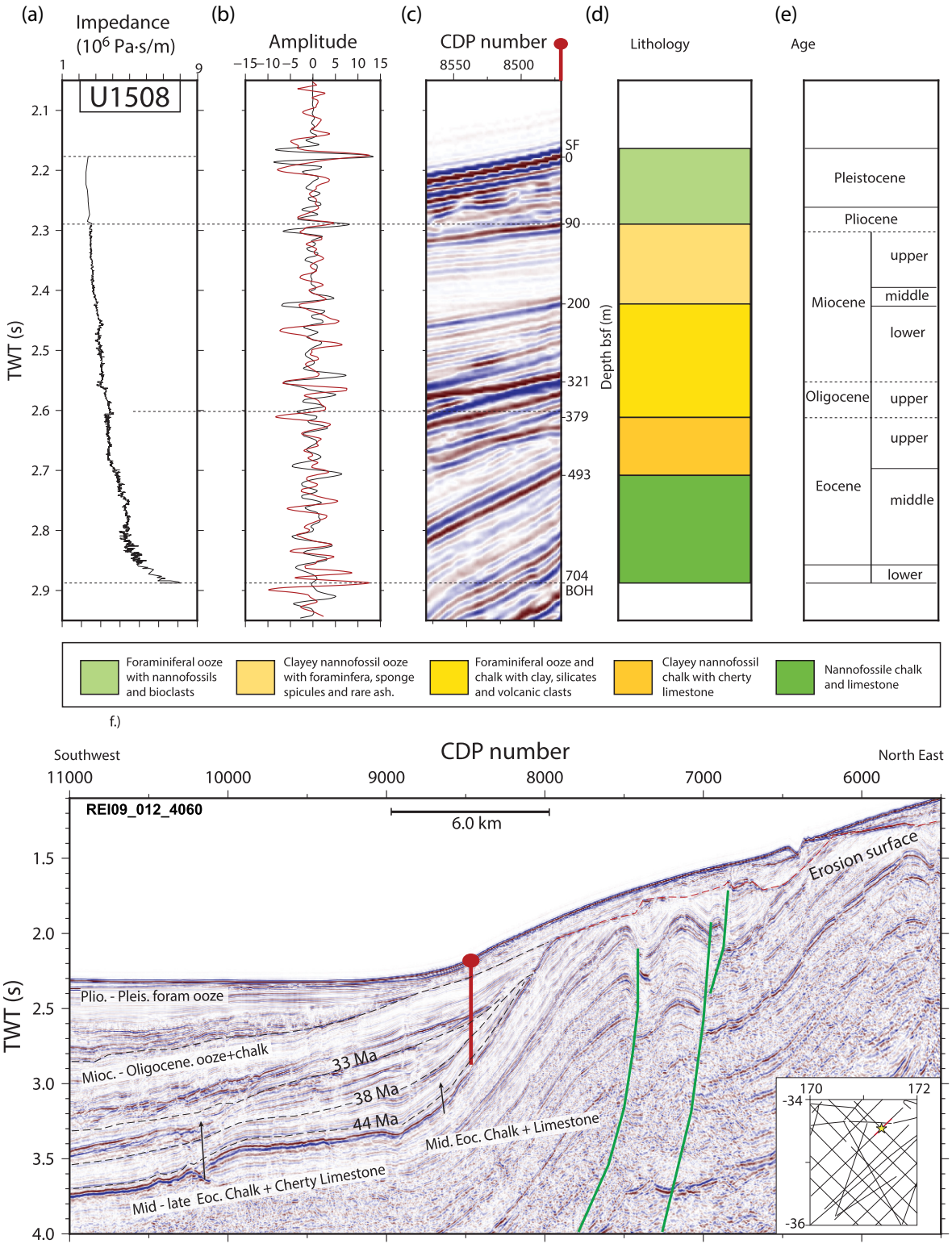

Figure 5. Borehole ties to seismic and timing of tectonic events at Site U1508. See the caption for Fig. 3 for further explanation. Green lines are fault traces.

3.1.6. Site U1511

Core measured *P*-wave velocity and density values are used to create the synthetic solution (Figs 2 and 8) at Site U1511. The borehole is cored between 0 and 70 m depth and between 200 and 500 m depth, with a drilled interval between. The velocity and density of the drilled section are estimated using an exponential velocity increase with depth. The top of the second cored section at 200 m depth is close to a lithological change that likely produces the

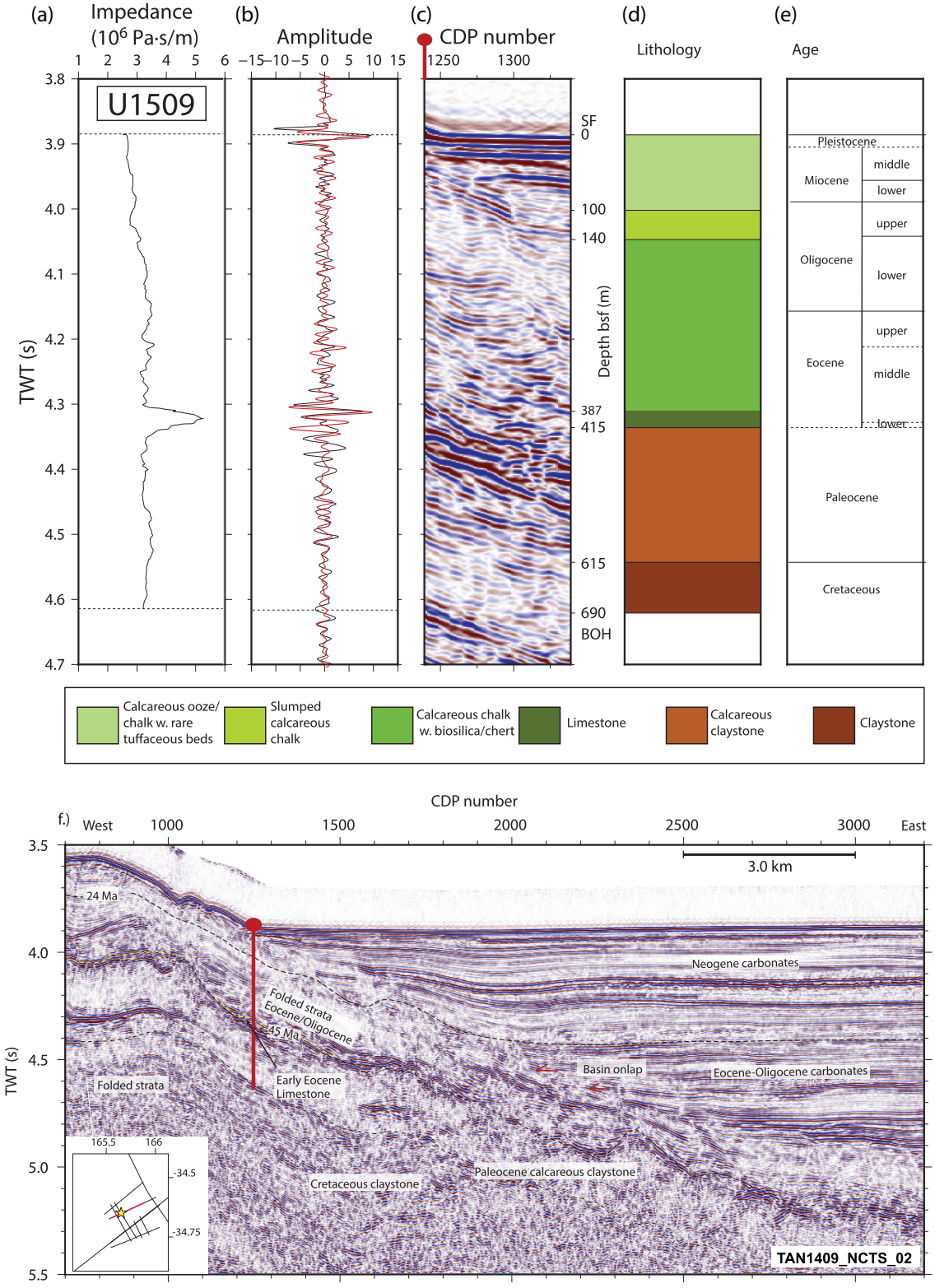

Figure 6. Borehole ties to seismic and timing of tectonic events at Site U1509. See the caption for Fig. 3 for further explanation.

negative polarity reflection observed at 6.7 s TWT on the multichannel data. However, the physical properties measured from the core do not constrain the velocity contrast across this reflector. A change in sediment composition from clay to diatomite is interpreted to coincide with the change in seismic character and a small sample of clay was recovered in the first core after the drilled interval (Sutherland et al. 2019). Forward modelling suggests that a velocity of ~1700 m s^{-1} is required at the base of the drilled section to replicate the amplitude of the negative polarity reflector from the boundary between clay and diatomite at ~200 m depth; a value

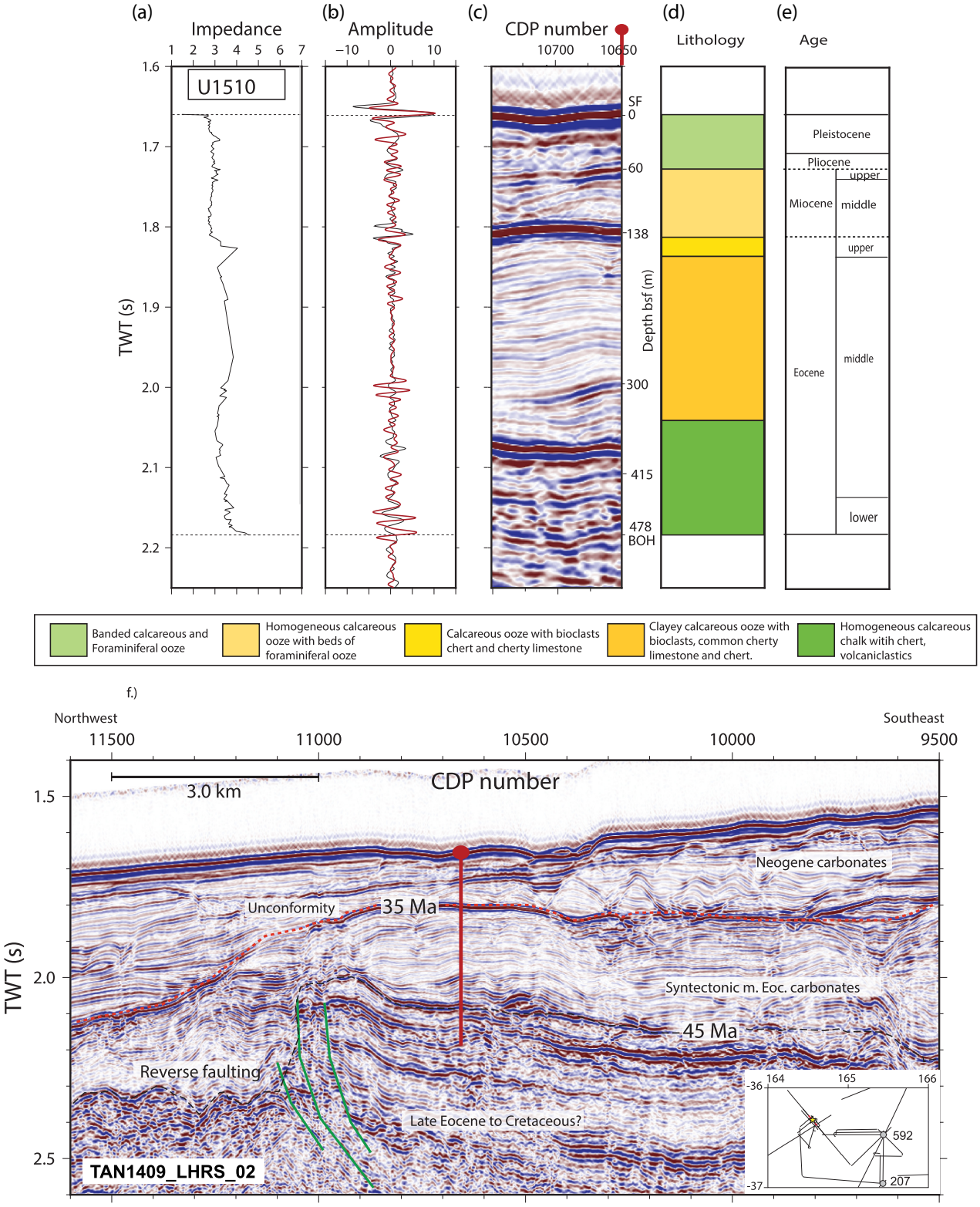

Figure 7. Borehole ties to seismic and timing of tectonic events at Site U1510. See the caption for Fig. 3 for further explanation.

appropriate for deep sea clay in this depth range (Carlson et al. 1986). A 3 per cent velocity correction is applied to the cored clay and diatomite sections. All major reflectors below the drilled section fit the synthetic solution produced using this corrected velocity.

The velocity with depth relationships for the synthetic models are used to produce numerical solutions for TWT with depth for seismic ties at the borehole sites (Fig. 9a).

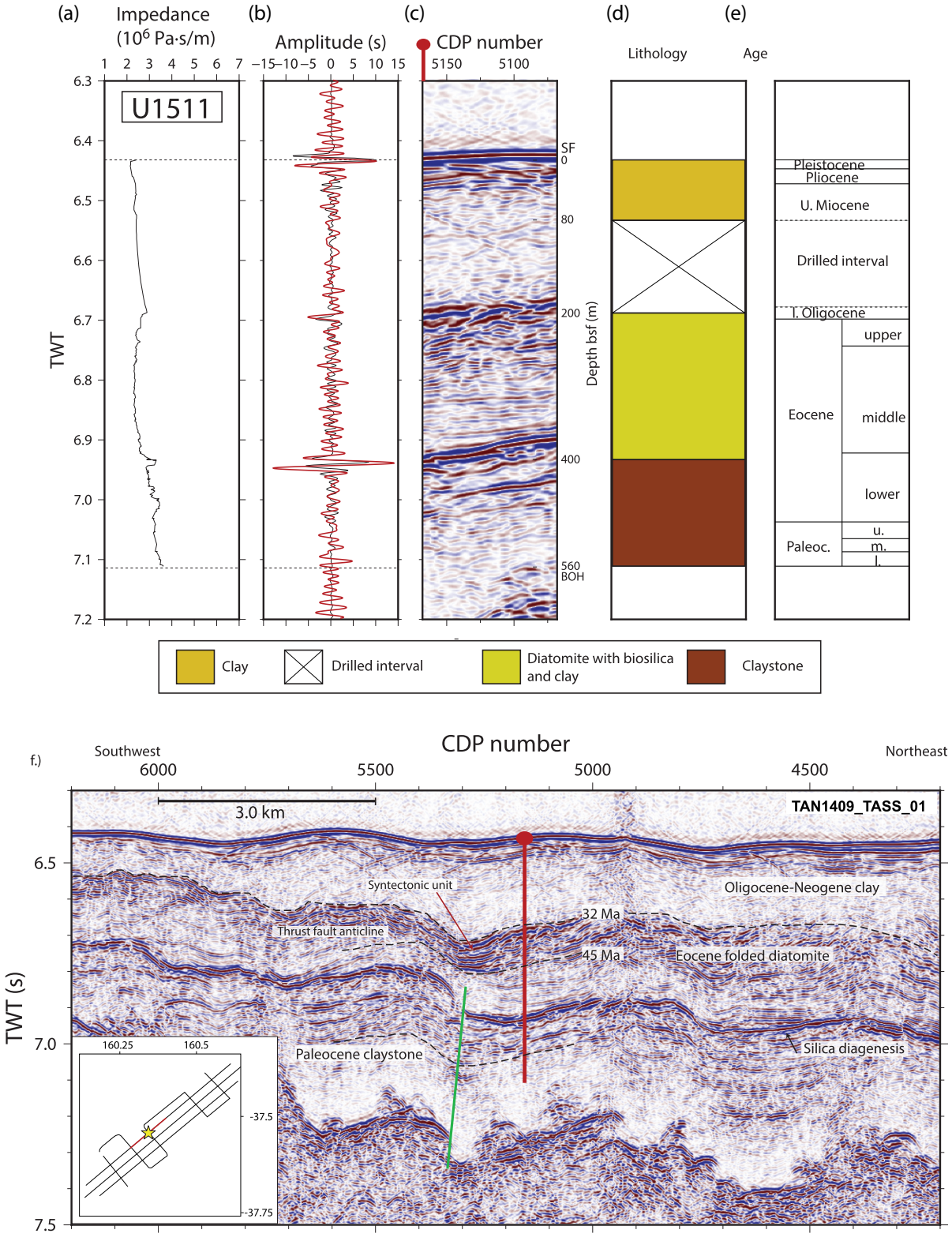

Figure 8. Borehole ties to seismic and timing of tectonic events at Site U1511. See the caption for Fig. 3 for further explanation. The silica diagenetic horizon, a possible bottom simulating reflection, crosscuts sediment layers and likely occurred during or after folding.

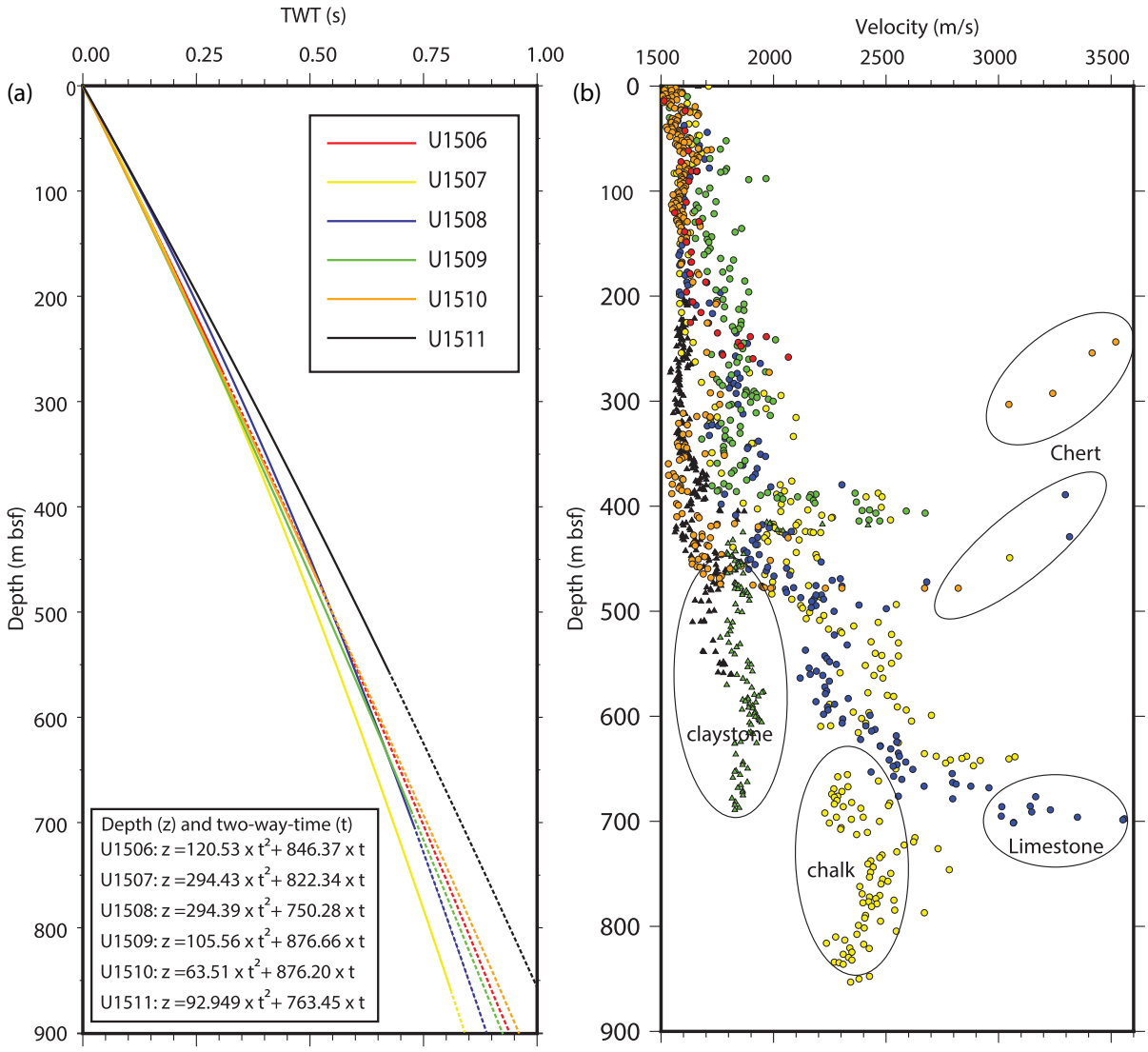

Figure 9. (a) TWT with depth relationship for the six IODP Expedition 371 boreholes. The core and wireline measured *P*-wave velocities are used to calculate these numerical solutions (see Section 3.1). Solid lines are constrained, and dashed lines are interpolated. *Inset:* numerical solution for TWT time with depth for each borehole. *The depth constrained in Site U1506 is the base of the sedimentary section in the borehole, volcanic basement is not included in the TWT calculation. Depths (*z*) are in metres bsf, TWT (t) is in seconds below the seafloor reflector. (b) Core measured velocities for the six boreholes with lithologies labelled where they can be grouped. Triangles are claystones and circles are carbonates with colours for each borehole given in (a). Labelled ellipses show the magnitude of the velocity differences between sediment types in the deeper parts of the boreholes.

3.2 Seismic velocities in northern Zealandia sediments

Core measured sediment velocities vary between 1500 and 3000 m s^{-1} with the highest velocities observed in carbonate with altered silica while lowest velocities are in deep sea diatomite (Fig. 2). Site U1506 on the northern Lord Howe Rise has the slowest velocities measured in carbonate in the Expedition 371 boreholes (Fig. 2a) over the depth range sampled [0–260 m below seafloor, (bsf)], which may be due to only trace amounts of terrigenous material or altered silicates and the relatively shallow water deposition at the site (Fig. 9b), all attributes that produce lower velocity carbonate (Anselmetti & Eberli 1993). On the southern Lord Howe Rise where water depths are also shallow, Site U1510 carbonate velocities are of comparable low velocity (Fig. 2e). Seismic velocities at the Site U1507 and U1508 boreholes (Figs 2b and c) are very similar indicating commonalities with the dominantly carbonate composition, fine-grained clay present and the largely deep-water, bathyal, setting for deposition. The TWT with depth solution at Site U1509 indicates slightly slower velocities (Fig. 2d) below 415 m bsf as the cored bathyal claystones are lower in velocity than the chalk found at similar burial depths at the other two deep-water bathyal sites (Sites U1507 and U1508, Fig. 9b).

The ooze to chalk transition in northern Zealandia is usually between 200 and 300 m bsf (from this study and DSDP sites summarized in Stratford et al. 2018) except at Sites U1509 and U1510 where it is 60 and 150 m, respectively. The shallower depths are attributed to the removal of overburden due to slumping on the margin of the New Caledonia Trough (Site U1509) and erosion on the Lord Howe Rise (Site U1510). The ooze to chalk transition is usually associated with decreased porosity and increased *Vp*, however the dominant effect on the regional variations in carbonate velocity in northern Zealandian sediments is attributed to the presence of clay, silica and volcaniclastics.

Abyssal clays containing diatomite at Site U1511 are the lowest velocity sediments measured across the boreholes (Figs 2f and 9a and b). These sediments have porosities as high as 80 per cent (Sutherland et al. 2019) and have *P*-wave velocities closer to those of water, ∼1600 m s^{-1}, down to 400 m bsf. These velocities are 400 m s^{-1} slower than those measured in carbonate at equivalent depths below the seafloor in northern Zealandia.

4 PALAEOGENE DEFORMATION IN THE SEDIMENTARY RECORD

4.1 Site U1506

Site U1506 was drilled on the northern Lord Howe Rise in a water depth of 1505 m, into a buried basement high visible in the multichannel data (Figs 3f and 10). Drilling revealed the basement high to be a basaltic volcano, which is yet to be dated. Volcanism related to rifting appears to have been common over the Lord Howe Rise during the Late Cretaceous with additional pulses of igneous and tectonic activity recorded in the post rift phase. Phases of Late Cretaceous to Eocene, late Oligocene to Miocene and Pliocene volcanism are inferred from dredge samples and interpreted using multichannel seismic data (Higgins et al. 2015). Stratigraphic relationships indicate that the basaltic volcano at Site U1506 likely dates from the Late Cretaceous to Eocene phase. A ∼270 m thick sequence of carbonate ooze and chalk overlie this basement. Most of the sedimentary sequence comprises middle Miocene and younger ooze, with 6 m of middle Oligocene chalk and 32 cm of middle Eocene glauconitic chalk. Unconformities separate the middle Eocene from middle Oligocene and the middle Oligocene from the Neogene section. No internal deformation is observed within the cored sediment at Site U1506, although channels and bedforms are visible in the seismic data indicating bottom current activity during the Neogene. The seismic section (Fig. 3f) shows an erosional unconformity as a strong negative polarity reflection between sediments deposited on the flanks of the volcano and the sediments that blanket it. The reflection is observed across the Lord Howe Rise in the region and is related to a change in sediment composition at the end of the Eocene (Stratford et al. 2018).

4.2 Site U1507

Site U1507 was drilled on the northeast side of the northern New Caledonia Trough (Fig. 1) in a water depth of ∼3500 m and terminated at 860 m bsf in middle Eocene carbonate (Figs 4f and 10). Synthetic modelling of borehole physical properties produced a good fit with the seismic trace for the site. Borehole ties to seismic data thus give sediment ages with a high degree of confidence. Sediments cored are carbonates that contain clay, with volcaniclastics and ash from the late Eocene. Deep reflectivity in the basin at the borehole site shows stratified layers in middle Eocene and older sediments. An unconformity and onlap sequence (at ∼5.5 s TWT, Fig. 4f) is interpreted as a middle Eocene facies change due to changes in sediment provenance (ridge sourced vs. basin) as no time gap was found in the core at this depth. The occurrence of volcaniclastics in the core coincide with the syntectonic unit and tilting of the flank of the Norfolk ridge toward the basin (Figs 4f and 10e). This late Eocene (∼36 Ma) to middle Miocene (15 Ma) tilting event is associated with progradation out from the ridge, high amplitude disrupted seismic reflectors and deposition of volcaniclastics that decrease in volume from the middle Oligocene. Post 15 Ma sediments are onlapping and volcanics are rare. A chain of seamounts is visible in the bathymetric data along the Norfolk Ridge up dip from the borehole site. Recent work has dated these as Eocene to Miocene in age and attributed them to mantle melting at a lithospheric step, with some possible influence of a subducted slab (Mortimer et al. 2021).

4.3 Site U1508

Site U1508 was drilled in a water depth of ∼1600 min Reinga Basin, ∼100 km northwest of the northern tip of New Zealand. The borehole terminated at 704 m bsf in lower Eocene limestone shown by a band of bright reflectivity on the multichannel seismic profile (Fig. 5f). The core comprises carbonate with the addition of bioclasts in the Pleistocene, silicates, clay and volcanics in the Miocene and Oligocene, and clay and chert in the Eocene. Shortening in the Reinga Basin occurred predominantly during the late Eocene between 38 and 33 Ma (Fig. 5f). Constraint from a network of seismic lines in the basin indicates that this compression event was widespread (Orr et al. 2020). Minor compression and slope failure likely continue into the Oligocene. The syntectonic unit comprises dipping sediments that were deposited during tilting of the edge of the basin on kilometre scale folds. Onlap onto these folded strata is observed on the margin of the basin with the deepest onlap horizon being the drilling target. Sediments in the borehole dip towards the basin below 475 m bsf and dips increase by only 5° between ∼38 to 44 Ma indicating negligible tilting occurred in the late middle Eocene (Sutherland et al. 2019).

The middle Eocene and older sediments are observed on seismic data as a unit of horizontally stratified sediment that has been incorporated into 10 km scale folds at the edge of the basin (Fig. 5). The late Eocene syntectonic unit (38 to 33 Ma) has a higher clay content, which may indicate erosion of nearby landmasses during tectonic shorting. Onlap continues into the Oligocene and Miocene near the borehole site at the edge of the basin although sediment dips decrease. These observations indicate a small degree of folding in the middle Eocene, a pronounced tectonic folding and uplift period in the late Eocene, with decreased folding and slope failure in the Oligocene and basin infill sedimentation with quiescence since the Pliocene.

The borehole terminated ∼40 ms above a bright, negative polarity reflector that can be traced regionally across Reinga Basin (Fig. 5f). Extrapolation below the borehole to the reflector using early Eocene sedimentation rates (Sutherland et al. 2019) gives an estimated age for the horizon as at or near the Palaeocene/Eocene boundary.

4.4 Site U1509

Site U1509 was drilled on the southern side of the New Caledonia Trough in a water depth of 2911 m and sampled Pleistocene to Cretaceous sediment (Figs 1 and 6). The depositional history at the borehole site is complex with basin margin slumping obscuring stratigraphic relationships and unconformities disrupting the stratigraphic record. Basin subsidence had begun by the Late Cretaceous (Etienne et al. 2017). The borehole terminated in Cretaceous claystone with carbonate content increasing up-core (Figs 6d and f), indicating bathyal deposition that became increasingly marine (∼1000 m water depth) by the end of the Palaeocene. A bright negative polarity reflector at the Palaeocene/Eocene boundary is also

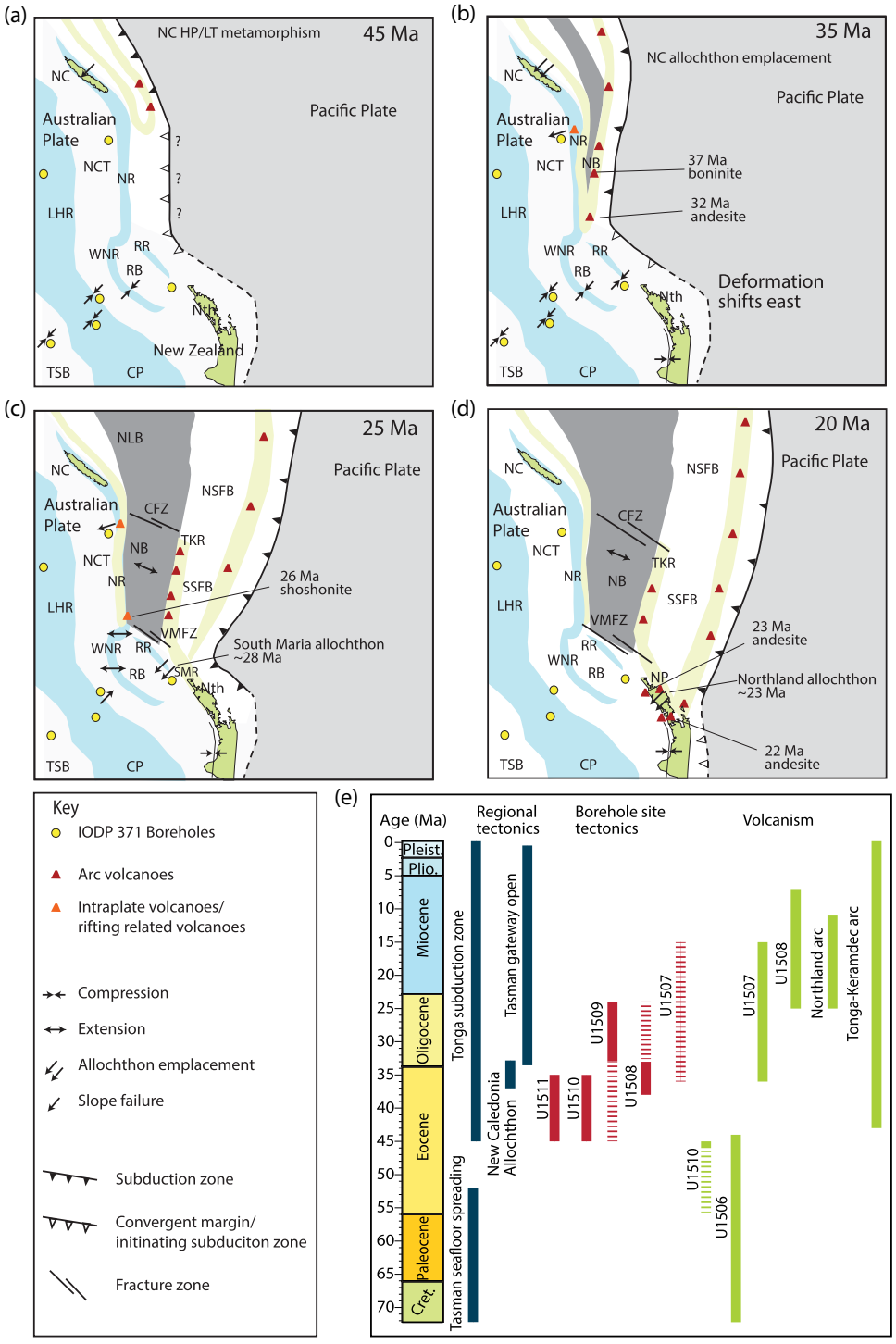

Figure 10. Cartoon summarizing the plate boundary and deformation evolution from the middle Eocene-Early Miocene. Red triangles are arc volcanoes. Orange triangles are volcanics related to rifting. NC is New Caledonia, NCT is New Caledonia Trough, NLB is North Loyalty Basin, SSFB is south South Fiji Basin, NSFB is north South Fiji Basin and TSB is Tasman Sea Basin. NR is Norfolk Ridge, WNR is West Norfolk Ridge, RR is Reinga Ridge, RB is Reinga Basin, VMFZ is Vening Meinesz Fracture Zone, CFZ is Cook Fracture Zone, NB is Norfolk Basin, TKR is Three Kings Ridge, LHR is Lord Howe Rise, CP is Challenger Plateau and Nth is Northland Peninsular. NP is Northland Plateau. Yellow dots show IODP 371 borehole sites. Convergence on the Taranaki fault is inferred to have started the middle Eocene (Stagpoole & Nicol 2008). Extension of the West Norfolk Ridge and emplacement of the South Maria Ridge Allochthon occur in the early Oligocene (~34–28 Ma, Orr et al. 2020). Norfolk Basin extension began around ~ 28 Ma (Herzer et al. 2011). The Northland Allochthon was emplaced onshore Northland from the NE in the early Miocene (Isaac et al. 1994; Rait 2000). (b) Summary of Cenozoic deformation and volcanic events in the southwest Pacific. Deformation ages at the borehole sites are plotted in red. The dashed part of the lines indicates when deformation is either poorly constrained or is less evident in the seismic data. Volcanic ages (Mortimer et al. 2007; Meffre et al. 2012) are plotted in green. The volcanics are labelled as 'arc' when they are inferred to be subduction related. Dashed parts of the lines indicate where there is no age constraint from borehole sampling, but ages are proposed from stratigraphic relationships.

observed where early Eocene limestones (Vp ~3000 m s^{-1}) overlie Palaeocene claystones (Vp ~2000 m s^{-1}, Fig. 6d). A change from shallow marine siliciclastic to marine pelagic sedimentation indicates deepening depositional environments (Boggs 1995) and a possible drowning of topography in the area. Tentative links between the top Palaeocene negative polarity reflector in southern New Caledonia Trough (Site U1509) and the one ~40 ms below the bottom of the borehole in Reinga Basin (Site U1508) may indicate that these reflectors mark regional changes in basin development and sediment provenance at the end of the Palaeocene.

The edge of the New Caledonia Trough is overprinted by Palaeogene shortening. Eocene to Oligocene reflectors onlap Palaeocene sediments at the edge of southern New Caledonia Trough (Fig. 6f), are deformed in basin edge folds and offset by slumping into the basin. The onset of the folding is difficult to date due to slumping of the margin, but likely started in the Eocene, becoming most pronounced from ~33 Ma. The end of deformation is better constrained at ~24 Ma, although this includes local slope failure that may have continued after deep-seated deformation ended. Fanning reflectors at the trough margin are visible in Oligocene sediments (33 to 24 Ma). Sediments were locally tilted during this phase of compression, rotating the geomorphic edge of the trough basin ward. The top of the folded sediments forms the new onlap surface for post Oligocene sediment accumulation in the trough. Water depths have been increasing since at least the Late Cretaceous, and the site represents a Cretaceous basin that has been overprinted by basin margin shortening that may have started in the Eocene (Etienne et al. 2017).

4.5 Site U1510

Site U1510 was drilled in a water depth of 1238 m on top of the southern Lord Howe Rise in an Eocene volcanic field (Fig. 1). The sediments cored are Pleistocene to lower Eocene carbonates with layers of chert and volcaniclastics in the middle Eocene (Figs 7d and f). No Oligocene sediments were recovered from the borehole with relatively thin Palaeogene sediments on the Lord Howe Rise compared to thicker sedimentary sequences off its flanks to the southwest. An unconformity separates the Miocene carbonate ooze from Eocene cherty chalk. The unconformity at the top of the Eocene syntectonic unit is shown on the seismic data as a bright reflector and coincidences with a chert layer in the borehole. Volcanic edifices can be seen on reconnaissance seismic lines in the area around the borehole and are blanketed by Neogene ooze. The Eocene syntectonic unit at Site U1510 has relatively high sedimentation rates with fanning reflectors adjacent to reverse faults and volcanic edifices (Fig. 7f). These sediments are deformed, and deeper sediments are offset by reverse faulting. Based on reflector geometry, the age of the syntectonic unit is between ~45 and 35 Ma. Early to middle Eocene (~46 Ma) volcaniclastics indicate that the nearby volcanic field was active just prior to the start of tectonic shortening. The youngest sediments below the unconformity are dated at 35 Ma, making this a maximum age for the end of deformation.

4.6 Site U1511

Site U1511 was drilled in the abyssal Tasman Sea Basin in a water depth of ~4900 m, ~100 km southwest of the Lord Howe Rise (Fig. 1). Magnetic anomaly interpretations indicate the oceanic crust beneath the borehole site is 74–84 Ma (palaeomagnetic Chron C33, Gaina et al. 1998) and the predominantly siliceous fossil evidence indicates the site has been below the CCD since the late Palaeocene. Sediments cored at the site are abyssal clay with the middle to late Eocene being rich in diatomite (Fig. 8). Short wavelength (~5 km), northeast verging asymmetric folds, offset on faults in places, deform Palaeogene sediments in this part of the Tasman Sea Basin and are recorded out to distances of ~100 km from the Lord Howe Rise margin. Palaeocene abyssal claystone contains bright bands of reflectivity whereas middle to late Eocene diatomite contains horizontally stratified low amplitude reflectivity and bright disturbed reflectivity. The overlying undeformed Neogene abyssal clay is largely opaque. At Site U1511 the syntectonic unit is a ~100 m thick layer marked by bright, disrupted reflectors that are truncated at the top and thicken away from anticline crests (Fig. 2f). Precisely dating the onset and termination of deformation at this site is hampered by the difficulty in laterally tracing intra-unit reflectors that indicate that the sediments deposited in an abyssal environment may have been subjected to bottom currents. The onset of deformation is interpreted to be after 45 Ma at the base of the layer of high reflectivity as parallel reflectors can be traced laterally below this depth. Folding is inferred to have ended by ~32 Ma at the top of the diatomite unit (Fig. 8f). The bright reflector in the Palaeocene claystone is a diagenetic horizon that mimics the shape of the folded Eocene layer. Opal CT, altered silica, was sampled in the borehole at a depth that correlates with this reflector (Sutherland et al. 2019).

5 PALAEOGENE PLATE TECTONICS

A complex period of subduction initiation in the western Pacific occurred during the period 53 to 43 Ma that included: the onset of arc volcanism in the Izu-Bonin-Mariana system (Arculus et al. 2015; Ishizuka et al. 2018); cessation of spreading in the Tasman Sea (Gaina et al. 1998); the onset of arc volcanism in the Tonga forearc (Meffre et al. 2012) (Fig. 1); formation of the Emperor-Hawaii bend (Torsvik et al. 2017), partially attributed to a change in direction of the Pacific plate (Whittaker et al. 2007); and onset of rapid seafloor spreading south of Australia and New Zealand that probably signifies a change in direction of the Australian plate (Sutherland 1995; Cande & Stock 2004). A period of tectonic adjustment after 45 Ma included the southward propagation towards New Zealand of the proto Tonga-Kermadec subduction zone, and the formation of backarc basins behind the system as it moved to the southeast forming the present-day Tonga-Kermadec-Hikurangi subduction margin (Fig. 10).

Our new constraints on the timing of failure of the Australian plate show that it occurred during this adjustment phase, after 45 Ma (Fig. 10). Three boreholes sites in the southern part of northern Zealandia (U1509, U1510 and U1511) indicate shortening beginning at this time (Figs 6–8). The observation of shortening out to distances ~1000 km from the evolving convergent margin indicates that the lithosphere of northern Zealandia in the Eocene was strong enough to act as a stress guide (Burov & Watts 2006). Observations from analogue models indicate that the transfer of stress to distances >1000km is possible where the downgoing and overriding plates are of similar strength (Leroy et al. 2004). Intraplate deformation has been recorded in the geological record in regions such as the North American craton (Marshak et al. 2004), the Arunta block in central Australia (Lambeck 1983) and northern Canada (Stephenson & Cloetingh 1991) and in oceanic lithosphere in the Indian Ocean (Bull et al. 1992; Beekman et al. 1996) at distances that exceed 1000 km from the plate margin.

Estimates of linear strain rate across the southern part of the study area range from 10^{-16} s^{-1} in Reinga Basin to 10^{-17}S^{-1} in the

Tasman Sea Basin. These values are estimated from the amount of shortening taken up by folding of sediment near the boreholes. The values are low in Reinga Basin compared to strain rates in basins behind the Tonga Kermadec subduction zone in New Zealand (Lamarche et al. 2005) in keeping with the low-plate convergence rates inferred in the Eocene (Bache et al. 2012) but the Tasman Basin values are comparable to the intraplate deformation values in central Australia, which is similarly ∼1000 km from active convergent margins (Lambeck 1983).

Evolution of the Tonga-Kermadec convergent margin during the early Palaeogene is not well resolved in northern Zealandia due to the scarce volcanic arc products sampled from this period. Rocks dredged from the Tonga Forearc indicate early Palaeogene arc volcanism occurred in the north near New Caledonia at ∼51 to 49 Ma (Meffre et al. 2012). Both northeast and southwest dipping subduction zones have been proposed with preference given to the rocks being from the backarc of a northeast dipping New Caledonia subduction zone that were transferred to the forearc of the southwest dipping Tonga-Kermadec subduction zone when polarity switched (Meffre et al. 2012). Subduction polarity is inferred to have switched during the attempted subduction of the buoyant Norfolk Ridge (Collot et al. 2008). Dolerites and rhyolites from the Tonga forearc dated at 43 to 39 Ma are interpreted as having originated in the newly formed Tonga-Kermadec subduction system that initiated following the change in subduction polarity (Meffre et al. 2012, Fig. 10a). Late Eocene (∼37 Ma) arc rocks have been dredged from the Three Kings Ridge (Mortimer et al. 2007, Fig. 10b), however opposing directions of subduction along this ridge in the Eocene have also been inferred (Kroenke & Dupont 1982; Herzer et al. 2000). Arc volcanics dredged from the Three Kings Ridge and South Fiji Basin are predominantly Miocene in age indicating an increase in productivity at the time southwest Pacific back arc basins were opening (Mortimer et al. 2007). In the absence of a clear volcanic arc, tectonic deformation dated from the initiation phase of the Tonga-Kermadec margin can shed light on the extent of the convergent margin at this time.

Formation of the proto Tonga-Kermadec subduction zone, along the northern margin of Zealandia in the middle Eocene is documented by ∼20 myr of convergent deformation recorded in Palaeogene marine sediments in the southern part of northern Zealandia. Although the two northern IODP Expedition 371 boreholes (Sites U1506 and U1507) do not indicate middle Eocene deformation, evidence for convergence in the north during this phase is indicated by shortening of basement and in sediments of the southern Coral Sea just off the coast of Australia (Fig. 1). Although undated, the age of the underlying oceanic crust (Gaina et al. 1998) indicates that this deformation is likely Palaeogene. The geological record of New Caledonia also contains varied evidence of Eocene tectonic shortening. Blue schist metamorphism starting in the early Eocene (Spandler et al. 2005), sediment composition changes from pelagic micrites to terrigenous-rich calciturbidites in the middle Eocene (Dallanave et al. 2018, 2020; Maurizot et al. 2020a; Bordenave et al. 2021, Fig. 10a) and ophiolite obduction in the late Eocene (Collot et al. 2020; Maurizot et al. 2020b, Fig. 10b) are attributed to the onset of different phases of convergent tectonics. Tectonic models for this time period invoke one or two subduction zones to the north east of New Caledonia (Matthews et al. 2015; Collot et al. 2020; Sutherland et al. 2020) but are generally in agreement that the proto Tonga-Kermadec subduction zone had initiated by middle Eocene, ∼45 Ma (Fig. 10a, Matthews et al. 2015; Collot et al. 2020).

Although dredged rocks indicate some Eocene arc activity along the Three Kings Ridge (Mortimer et al. 2007) no arc rocks have been sampled from north of Reinga Basin (Fig. 1). Little geological information is available to constrain the Eocene plate margin here as the region now comprises ocean basins formed since the Miocene (Fig. 1, Herzer et al. 2004; Mortimer et al. 2007). The deformation documented in this study may be the only source of structural evidence for the plate boundary along this part of the margin at the time.

The folding of Cretaceous to early Eocene sediments on the north side of Reinga Basin between 38 and 33 Ma (Fig. 10b), indicates a convergent margin was just northwest of New Zealand by the late Eocene. Deformation is observed at sites that are both proximal (Sites U1508) and distal (Sites U1509, U1510 and U1511) to the boundary (Figs 1 and 10) indicating strain accumulation over large distances. The direction of maximum principal compressive stress is estimated to be approximately northeast–southwest (Fig. 10), although, deformation is accommodated by the reactivation of pre-existing abyssal hill and Cretaceous rift faults (Bache et al. 2012), there is some scatter. Low convergence rates (<20 mm yr^{-1}) between the Pacific and Australian plates are indicated by the position of the rotation pole (Fig. 1), which may explain why Eocene or Oligocene arc volcanic products have not been found in this part of northern Zealandia (Sutherland 1995; Ballance 1999; Mortimer et al. 2007; Bache et al. 2012). Approximately 150 km of convergence is required to produce arc volcanism and the inference is that convergence across this boundary may have been insufficient to produce self-sustaining mature subduction and arc volcanism (Gurnis et al. 2004). As a result of the opening of the South Fiji Basin the structural features of the Eocene convergent margin may now lie offshore Northland New Zealand, where no Palaeogene volcanic products have been sampled (Mortimer et al. 2007).

The late Eocene to Miocene tilting at the northern New Caledonia Trough borehole Site U1507 is contemporaneous with volcaniclastics likely sourced from volcanoes observed on the Norfolk Ridge up dip from the borehole (Figs 10b and e). There is a switch from compressional to extensional tectonics behind the subduction system in the north at this time (Fig. 10b). The geochemistry of the volcanoes indicates that they are most likely intraplate in origin (Mortimer et al. 2021) but with possible input from a subducted slab. The borehole site is behind the Norfolk Basin and tilting of the northern side of the New Caledonia Trough may be linked to regional extensional tectonics or backarc processes behind the Three-Kings Ridge part of the Tonga-Kermadec margin, which preceded the opening of the Norfolk basin during the early Miocene (Mortimer et al. 2010).

Around ∼25 Ma the pole of rotation shifted to the southeast (Fig. 1, Sutherland 1995; Ballance 1999). Extension began in the Norfolk Basin and West Norfolk Ridge (Herzer et al. 2011; Orr et al. 2020) and the Southern New Caledonia Trough and Reinga basin borehole sites show slope failure (Fig. 10c). Plate convergence rates increased in the region and the Three Kings Ridge moved eastward by dextral translation on the Vening Meinesz fracture zone during Norfolk Basin opening (Herzer et al. 2009, 2011, Figs 1 and 10). The South Maria Allochthon was emplaced onto South Maria Ridge in the Oligocene (Fig. 10c) with the Northland Allochthon being emplaced around ∼5–11 Ma later in the early Miocene (Isaac et al. 1994; Orr et al. 2020; Rait 2000, Fig. 10d). The opening of the South Fiji Basin began translating the Tonga-Kermadec trench eastward (Fig. 10d) towards its present-day location north of New Zealand (Mortimer et al. 2007) coinciding with the end of the compressive phase observed in northern Zealandian sediments. In the Miocene, there was a further shift in the plate rotation pole position to the

southeast, subduction began north of New Zealand with the Hikurangi subduction zone established by the middle Miocene (Raitt et al. 1991).

IODP Expedition 371 borehole age constraints of convergent deformation presented here shed light on Eocene tectonics in northern Zealandia during the period of early evolution of what would become the Tonga-Kermadec subduction zone. Deformation observed in southern Zealandia sediments indicates a convergent boundary was established along the northern Zealandian margin in the middle Eocene and was as far south as Reinga Basin by the late Eocene. Although the initiation phase of the western Pacific subduction slabs may have been comparatively rapid (Whittaker et al. 2007; Arculus et al. 2015; Seton et al. 2015; Reagan et al. 2019; Mauder et al. 2020), development of a mature subduction zone capable of arc magmatism may have taken some time in the southwest Pacific.

6 SUMMARY

New borehole physical property data from northern Zealandia collected during IODP Expedition 371 are used to convert between depth and two-way traveltime on multichannel seismic data. Deformed and undeformed strata interpreted from seismic data can hence be tied to age–depth data at boreholes and used to determine the timing of intraplate failure that occurred ∼1000 km behind the initiating Tonga-Kermadec subduction system. The observed phase of intraplate deformation started during the middle Eocene at ∼45 Ma and was largely complete by the end of the Eocene. Deformation may have locally continued into the Oligocene, possibly as late as ∼24 Ma on the west flank of New Caledonia Trough, where local slope failure may have also contributed to the deformation signal.

Convergent deformation is observed in the southern part of the study area: Reinga Basin (Site U1508), southern New Caledonia Trough (Site U1509), southern Lord Howe Rise (Site U1510) and the Tasman Sea Basin (Site U1511). Northern Lord Howe Rise (Site U1506) and northern New Caledonia Trough (Site U1507) do not contain deformation that can be directly linked to subduction initiation however the geological record of New Caledonia indicates convergent tectonics in the north at this time.

A period of rapid early Eocene subduction initiation in the western Pacific was followed by a period of tectonic adjustment after 45 Ma that included the southward propagation of the Tonga-Kermadec subduction zone, and the formation of backarc basins behind the system as it moved to the southeast forming the present-day Tonga-Kermadec-Hikurangi subduction margin. Our new age constraints indicate a convergent margin north of Zealandia and failure of the Australian plate after ∼45 Ma. Compressive stresses may have developed during the initiation and the southward propagation of the proto Tonga-Kermadec subduction system which is temporally linked to the phase of stress that caused intraplate folding and faulting behind the evolving margin.

ACKNOWLEDGMENTS

We thank the International Ocean Discovery Program (IODP); the onboard personnel of R/V JOIDES Resolution on Expedition 371; shore-based proponents; and the scientists who conducted the site surveys on voyage TAN1409. This work was funded by the U.S. National Science Foundation; IODP participating countries; New Zealand, France, and New Caledonia. MG was supported by the National Science Foundation (OCE-2049086). LA acknowledges support from project PID2019-105537RB-I00 (Spanish Ministry of Science and Innovation and FEDER funds) and a 2017 Leonardo Grant for Researchers and Cultural Creators, BBVA Foundation. MG thanks the Coordenação de Aperfeiçoamento de Pessoal de Nível Superior—Brasil (CAPES)—that granted his participation in the IODP Expedition 371″. ED is supported by Deutsche Forschungsgemeinschaft (DFG; German research foundation)—projektnummer 408178503. H-HH acknowledges support from Japan Agency for Marine-Earth Science and Technology and Peter Buck Postdoctoral Fellowship of the National Museum of Natural History, Smithsonian Institution. We thank Ron Hackney and an anonymous reviewer for the helpful edits and suggestions that have improved the manuscript.

DATA AVAILABILITY

Seismic reflection data were compiled into an available database resource (Sutherland et al. 2012) and can be obtained from GNS Science (data.gns.cri.nz/pbe) or NZ Petroleum and Minerals (data.nzpam.govt.nz). International Ocean Discovery Program Expedition 371 borehole data are available via IODP's LIMS online report portal website https://web.iodp.tamu.edu/LORE/. Borehole velocity and density models and examples of tested borehole tie to seismic models are available from the data repository, https://zenodo.org/badge/latestdoi/436458689.

REFERENCES

Anselmetti, F.S. & Eberli, G.P., 1993. Control on sonic velocity in carbonates, *Pure appl. Geophys.,* **141,** 287–323.

Arculus, R.J. *et al.* 2015. A record of spontaneous subduction initiation in the Izu–Bonin–Mariana arc, *Nat. Geosci.,* **8,** 728–733.

Bache, F., Mortimer, N., Sutherland, R., Collot, J., Rouillard, P., Stagpoole, V. & Nicol, A., 2014. Seismic stratigraphic record of transition from Mesozoic subduction to continental breakup in the Zealandia sector of eastern Gondwana, *Gondwana Res.,* **26,** 1060–1078.

Bache, F., Sutherland, R., Stagpoole, V., Herzer, R.H., Collot, J. & Rouillard, P., 2012. Stratigraphy of the southern Norfolk Ridge and the Reinga Basin: a record of initiation of Tonga-Kermadec-Northland subduction in the southwest Pacific, *Earth planet. Sci. Lett.,* **321-322,** 41–53.

Ballance, P., 1999. Simplification of the Southwest Pacific Neogene arcs: inherited complexity and control by a retreating pole of rotation. *in Continental Tectonics,* pp. 7–19, eds Mac Niocaill, C. & Ryan, P. D. Geological Society Special Publications.

Beekman, F., Bull, J.M., Cloetingh, S. & Scrutton, R.A., 1996. Crustal fault reactivation facilitating lithospheric folding/buckling in the central Indian Ocean, *Geol. Soc., Lond., Spec. Publ.,* **99,** 251.

Boggs, S., 1995. *Principles of Sedimentology and Stratigraphy,* 2rd ed., Upper Saddle River, N.J.: Prentice Hall.

Bordenave, A. *et al.* 2021. Upper Cretaceous to Palaeogene successions of the Gouaro anticline: deepwater sedimentary records of the tectonic events that led to obduction in New Caledonia (SW Pacific), *Sediment. Geol.,* **415,** 105818.

Bradshaw, J.D., 1989. Cretaceous geotectonic patterns in the New Zealand region., *Tectonics,* **8,** 803–820.

Bull, J., Martinod, J. & Davy, P., 1992. Buckling of the oceanic lithosphere from geophysical data and experiments, *Tectonics,* **11,** 537–548.

Burns, R.E. *et al.*, 1973. Site 208. Texas A & M University, Ocean Drilling Program, College Station, TX, United States, pp. 271–281.

Burov, E.B., 2010. The equivalent elastic thickness (Te), seismicity and the long-term rheology of continental lithosphere:time to burn-out "creme brulee? Insights from large-scale geodynamic modeling., *Tectonophysics,* **484,** 4–26.

Burov, E.B. & Watts, A.B., 2006. The long-term strenght of the coninental lithosphere: 'jelly sandwich' or 'creme brulee'?, *GSA Today,* **16,** 4–10.

Cande, S.C. & Stock, J.M., 2004. Pacific - Antarctic-Australian motion and the formation of the Macquarie Plate, *Geophys. J. Int.,* **157,** 399–414.

Carlson, R.L., Gangi, A.F. & Snow, K.R., 1986. Empirical reflection travel time versus depth and velocity functions for the deep-sea sediment column, *J. geophys. Res.,* **91,** 8249–8266.

Chen, Y., Wu, J. & Suppe, J., 2019. Southward propagation of Nazca subduction along the Andes, *Nature,* **565,** 441–447.

Collot, J., Geli, L., Lafoy, Y., Vially, R., Cluzel, D., Klingelhoefer, F. & Nouze, H., 2008. Tectonic history of northern New Caledonia Basin from deep offshore seismic reflection: relation to late Eocene obdcution in New Caledonia, southwest Pacific, *Tectonics,* **27,** n/a.

Collot, J. *et al.*, 2020. Chapter 2 Geodynamics of the SW Pacific: a brief review and relations with New Caledonian geology, *Geol. Soc. Lond., Mem.,* **51,** 13–26.

Crawford, A.J., Meffre, S. & Symonds, P.A., 2003. 120-0 Ma tectonic evolution of southwest Pacific and analogous geological evolution of the 600 to 220 Ma Tasman Fold Belt System, *Geol. Soc. Australia*(Spec. Publ.) 377–397.

Dallanave, E. *et al.*, 2018. Magneto-biostratigraphic constraints of the Eocene micrite–calciturbidite transition in New Caledonia: tectonic implications, *N.Z. J. Geol. Geophys.,* **61,** 145–163.

Dallanave, E. *et al.*, 2020. Eocene (46-44 Ma) onset of Australia-Pacific plate motion in the southwest Pacific inferred from stratigraphy in New Caledonia and New Zealand, *Geochem. Geophys. Geosyst.,* **21,** 1–23.

Etienne, S. *et al.*, 2017. Deepwater sedimentation and Cenozoic deformation in the Southern New Caledonia Trough (Northern Zealandia, SW Pacific), *Mar. Pet. Geol.,* **92,** 764–779.

Gaina, C., Mueller, D.r., Royer, J.-Y., Stock, J., Hardebeck, J.L. & Symonds, P., 1998. The tectonic history of the Tasman Sea; a puzzle with 13 pieces, *J. geophys. Res.,* **103,** 12413–12433.

Gallais, F., Fujie, G., Boston, B., Hackney, R., Kodaira, S., Miura, S., Nakamura, Y. & Kaiho, Y., 2019. Crustal structure across the Lord Howe Rise, Northern Zealandia, and rifting of the eastern Gondwana margin, *J. geophys. Res.,* **124,** 1–21.

Gradstein, F.M., Ogg, J.G., Schmitz, M.D. & Ogg, G.M.E., 2012. *The Geological Time Scale 2012,* Amsterdam (Elsevier).

Gurnis, M., Hall, C. & Lavier, L., 2004. Evolving force balance during incipient subduction, *Geochem. Geophys. Geosyst.,* **5,** 1–31.

Handy, M.R. & Brun, J.P., 2004. Seismicity, structure and strenght of the continental lithosphere, *Earth planet. Sci. Lett.,* **223,** 427–441.

Herzer, R., Davy, B.W., Mortimer, N., Quilty, P., Chaproniere, G., Jones, C.M., Crawford, A.J. & Hollis, C.J., 2009. Seismic stratigraphy and structure of the Northland Plateau and the development of the Vening Meinesz transform margin, SW Pacific Ocean, *Mar. Geophys. Res.,* **30,** 21–60.

Herzer, R., Mascle, J., Davy, B., Ruellan, E., Mortimer, N., Laporte, C. & Duxfield, A., 2000. New constraints on the New Zealand–South Fiji Basin continent-back-arc margin, *C. R. Acad. Sci.—Ser. IIA—Earth Planet. Sci.,* **330,** 701–708.

Herzer, R., Mortimer, N., Davy, B., Barker, H. D. & Quilty, P., 2004. *Geology and Structure of the Southern End of the South Fiji Basin,* SW Pacific Ocean.

Herzer, R.H., Barker, D.H.N., Roest, W.R. & Mortimer, N., 2011. Oligocene-Miocene spreading history of the northern South Fiji Basin and implications for the evolution of the New Zealand plate boundary, *Geochem. Geophys. Geosyst.,* **12**.

Higgins, K. *et al.*, 2015. Structural analysis of extended Australian continental crust: capel and Faust basins, Lord Howe Rise. in *Sedimentary Basins and Crustal Processes at Continental Margins: From Modern Hyper-extended Margins to Deformed Ancient Analogues,* pp. 0 Geological Society of London.

Isaac, M.J., Herzer, R.H., Brook, F.J. & Hayward, B.W., 1994. *Cretaceous and Cenozoic Basins of Northland,* New Zealand, Institute of Geological and Nuclear Sciences Monograph,p. 8.

Ishizuka, O. *et al.*, 2018. Age of Izu–Bonin–Mariana arc basement, *Earth planet. Sci. Lett.,* **481,** 80–90.

Klingelhoefer, F., Lafoy, Y., Collot, J., Cosquer, E., Geli, L., Nouze, H. & Vially, R., 2007. Crustal structure of the basin and ridge system west of New Caledonia (southwest Pacific) from wide-angle and reflection seismic data, *J. geophys. Res.,* **112,** B11102.

Kroenke, L.W. & Dupont, J., 1982. Subduction-obduction: a possible north-south transition along the west flank of the Three Kings Ridge, *Geo Mar. Lett.,* **2,** 11–16.

Lamarche, G., Proust, J.-N. & Nodder, S.D., 2005. Long-term slip rates and fault interactions under low contractional strain, Wanganui Basin, New Zealand, *Tectonics,* **24,** TC4004.

Lambeck, K., 1983. Structure and evlotuio ofhe intracratonic basins of central Australia., *Geophys. J. R. astr. Soc.,* **74,** 843–886.

Leng, W. & Gurnis, M., 2011. Dynamics of subduction initiation with different evolutionary pathways, *Geochem. Geophys. Geosyst.,* **12,** Q12018.

Leroy, M., Dauteuil, O. & Cobbold, P.R., 2004. Incipient shortening of a passive margin: the mechanical roles of continental and oceanic lithospheres, *Geophys. J. Int.,* **159,** 400–411.

Lewis, S.D. & Hayes, D.E., 1983. The tectonics of northward propagating subduction along Eastern Luzon, Philippine Islands, *Geophys. Monogr. Ser.,* **27,** 57–78.

Li, H. *et al.*, 2021. Basalt derived from highly refractory mantle sources during early Izu-Bonin-Mariana arc development, *Nat. Commun.,* **12,** 1723.

Marshak, S., Karlstom, K. & Timmons, J.M., 2004. Inversion of Proterozoic extensional faults: an explanation for the pattern of Laramide and Ancestral Rockies intracratonic deformation, United States, *Geology,* **28,** 735–738.

Matthews, K.J., Williams, S.E., Whittaker, J.M., Muller, R.D., Seton, M. & Clarke, G., 2015. Geologic and kinematic constraints on Late Cretaceous to mid Eocene plate boundaries in the southwest Pacific, *Earth Sci. Rev.,* **140,** 72–107.

Mauder, B., Prytulak, J., Goes, S. & Reagan, M., 2020. Rapid subduction initiation and magmatism in the Western Pacific driven by internal vertical forces, *Nat. Commun.,* **11,** 1–8.

Maurizot, P., Bordenave, A., Cluzel, D., Collot, J. & Etienne, S., 2020a. Chapter 4 Late Cretaceous to Eocene cover of New Caledonia: from rifting to convergence, *Geol. Soc., Lond. Mem.,* **51,** 53–91.

Maurizot, P. *et al.*, 2020b. Chapter 5 The Eocene subduction–obduction complex of New Caledonia, *Geol. Soc. Lond., Mem.,* **51,** 93–130.

Meffre, S., Falloon, T.J., Crawford, T.J., Hoernle, K., Hauff, F., Duncan, R.A., Bloomer, S.H. & Wright, D.J., 2012. Basalts erupted along the Tongan forearc during subduction initiation: evidence from geochronology of dredged rocks from the Tonga forearc and trench, *Geochem. Geophys. Geosyst.,* **13,** 1–17.

Mortimer, N., Gans, P.B., Palin, J.M., Meffre, S., Herzer, R.H. & Skinner, D.N.B., 2010. Location and migration of Miocene–Quaternary volcanic arcs in the SW Pacific region, *J. Volc. Geotherm. Res.,* **190,** 1–10.

Mortimer, N., Herzer, R., Gans, P.B., Laporte-Magoni, C., Calvert, A.T. & Bosch, D., 2007. Oligocene-Miocene tectonic evolution of the South Fiji Basin and Northland Plateau, SW Pacific Ocean: evidence from petrology and dating of dredged rocks., *Mar. Geol.,* **237,** 1–24.

Mortimer, N. *et al.*, 2021. The Norfolk Ridge seamounts: eocene–Miocene volcanoes near Zealandia's rifted continental margin, *Aust. J. Earth Sci.,* **68,** 368–380.

Müller, R.D. *et al.*, 2016. Ocean basin evolution and global-scale plate reorganization events since Pangea breakup, *Annu. Rev. Earth Planet. Sci.,* **44,** 107–138.

Orr, D., Sutherland, R. & Stratford, W.R., 2020. Eocene to Miocene subduction initiation recorded in stratigraphy of Reinga Basin, northwest New Zealand, *Tectonics,* **39,** e2019TC005899.

Ozawaa, A., Tagamia, T., Listancob, E.L., Arpac, C.B. & Sudod, M., 2004. Initiation and propagation of subduction along the Philippine Trench: evidence from the temporal and spatial distribution of volcanoes, *J. Asian Earth Sci.,* 104–111.

Pirera, F. & Zanzi, L., 1993. The reflectivity method as a tool for evaluating the seismic response of layered structures, *J. appl. Geophys.,* **30,** 35–41.

Raimondo, T., Hand, M. & W.J., C., 2014. Compressional intracontinental orogens: ancient and modern perspectives, *Earth Sci. Rev.,* **130,** 128–153.

Rait, G.J., 2000. Thrust transport directions in he Northland Allocthon, New Zealand, *N.Z. J. Geol. Geophys,* **43,** 271–288.

Raitt, G., Chanier, F. & Waters, D.W., 1991. Landward-and seaward-directed thrusting accompanying the onset of subduction beneath New Zealand, *Geology,* **19,** 230–233.

Reagan, M.K., Heaton, D.E., Schmitz, M.S., Pearce, J.A., Shervais, J.W. & Koppers, A.P., 2019. Forearc ages reveal extensive short-lived and rapid seafloor spreading following subduction initiation, *Earth planet. Sci. Lett.,* **506,** 520–529.

Ricker, N., 1943. Further developments in the wavelet theory of seismogram structure, *Bull. seism. Soc. Am.,* **33,** 197–228.

Schellart, W.P., 2006. A late Cretaceous and Cenozoic reconstruction of the Southwest Pacific region: tectonics controlled by subduction and slab rollback processes, *Earth Sci. Rev.,* **76,** 191–233.

Schellart, W.P. & Spakman, W., 2012. Mantle constraints on the plate tectonic evolution of the Tonga–Kermadec–Hikurangi subduction zone and the South Fiji Basin region, *Aust. J. Earth Sci.,* **59,** 933–952.

Seton, M., Flament, N., Whittaker, J., Müller, R.D., Gurnis, M. & Bower, D.J., 2015. Ridge subduction sparked reorganization of the Pacific plate-mantle system 60–50 million years ago, *Geophys. Res. Lett.,* **42,** 1732–1740.

Spandler, C., Rubatto, D. & Hermann, J., 2005. Late Cretaceous-Tertiary tectonics of the southwest Pacific: insights from U-Pb sensitive, high-resolution ion microprobe (SHRIMP) dating of eclogite facies rocks from New Caledonia, *Tectonics,* **24,** TC3003.

Stagpoole, V. & Nicol, A., 2008. Regional structure and kinematic history of a large subduction back thrust: taranaki Fault, New Zealand, *J. geophys. Res.: Solid Earth,* **113,** B01403.

Stephenson, R.A. & Cloetingh, S.A.P.L., 1991. Some examples and mechanical aspect of continental lithopsheric folding, *Tectonophysics,* **188,** 27–37.

Stern, R.J., 2004. Subduction initiation: spontaneous and induced, *Earth planet. Sci. Lett.,* **226,** 275–292.

Stern, R.J. & Gerya, T., 2018. Subduction initiation in nature and models: a review, *Tectonophysics,* **746,** 173–198.

Stratford, W.R., Sutherland, R. & Collot, J., 2018. Physical properties and seismic-reflection interpretation of bathyal marine sediments affected by carbonate and silica diagenesis in the Tasman Sea, *N.Z. J. Geol. Geophys.,* **61**(1), 96–111.

Sutherland, R., 1995. The Australian-Pacific plate boundary and Cenozoic plate motion in the Pacific: some constraints from Geosat data, *Tectonics,* **14,** 819–831.

Sutherland, R. *et al.*, 2019. *Tasman Frontier Subduction Initiation and Paleogene Climate Proceedings of the International Ocean Discovery Program,* **371,** College Station, TX, International Ocean Discovery Program.

Sutherland, R. *et al.*, 2020. Continental-scale geographic change across Zealandia during Paleogene subduction initiation, *Geology,* **48,** 419–424.

Sutherland, R. *et al.*, 2012. *Compilation of Seismic Reflection Data from the Tasman Frontier region, Southwest Pacific,* 72p., ed 2012/01, G. S. R.

Torsvik, T.H., Doubrovine, P.V., Steinberger, B., Gaina, C., Spakman, W. & Domeier, M., 2017. Pacific plate motion change caused the Hawaiian-Emperor Bend, *Nat. Commun.,* **8,** 15660.

Urmos, J. & Wilkens, R.H., 1993. In situ velocities in pelagic carbonates: new insights from Ocean Drilling Program Leg 130, Ontong Java Plateau, *J. geophys. Res.,* **98,** 7903–7920.

Uruski, C., 2010. New Zealand's deepwater frontier,*Mar. Pet. Geol.,* **27,** 2005–2026.

Whattam, S.A., Malpas, J., Ali, J.R. & Smith, I., 2008. New SW Pacific tectonic model: cyclical intraoceanic magmatic arc construction and near-coeval emplacement along the Australia-Pacific margin in the Cenozoic, *Geochem. Geophys. Geosyst.,* **9,** n/a–n/a.

Whittaker, J.M., Muller, R.D., Leitchenkov, G., Stagg, H., Sdrolias, M., Gaina, C. & Goncharov, A., 2007. Major Australian-Antarctic plate reorganization at Hawaiian-Emperor bend time, *Science,* **318,** 83–86.

Wood, R.A., Herzer, R.H., Sutherland, R. & Melhuish, A., 2000. Cretaceous-Tertiary tectonic history of the Fiordland margin, New Zealand, *N. Z. J. Geol. Geophys.,* **43,** 289–302.

Zhou, X., Li, Z.-H., Gerya, T., Stern, R.J., Xu, Z. & Zhang, J., 2018. Subduction initiation dynamics along a transform fault control trench curvature and ophiolite ages, *Geology,* **46,** 607–610.